JGR Atmospheres

RESEARCH ARTICLE
10.1029/2019JD030502

Special Section:
The Arctic: An AGU Joint Special Collection

Impacts of Representing Heterogeneous Distribution of Cloud Liquid and Ice on Phase Partitioning of Arctic Mixed-Phase Clouds with NCAR CAM5

Meng Zhang[1,2], Xiaohong Liu[1,2], Minghui Diao[3], John J. D'Alessandro[4], Yong Wang[5], Chenglai Wu[6], Damao Zhang[7], Zhien Wang[8], and Shaocheng Xie[9]

[1]Department of Atmospheric Science, University of Wyoming, Laramie, WY, USA, [2]Now at Department of Atmospheric Sciences, Texas A&M University, College Station, Texas, USA, [3]Department of Meteorology and Climate Science, San Jose State University, San Jose, CA, USA, [4]Cooperative Institute for Mesoscale Meteorological Studies, University of Oklahoma, Norman, OK, USA, [5]Department of Earth System Science, Tsinghua University, Beijing, China, [6]International Center for Climate and Environment Sciences, Institute of Atmospheric Physics, Chinese Academy of Sciences, Beijing, China, [7]Brookhaven National Laboratory, Upton, NY, USA, [8]Department of Atmospheric and Oceanic Sciences, University of Colorado Boulder, Boulder, CO, USA, [9]Lawrence Livermore National Laboratory, Livermore, CA, USA

Abstract In this study, we conduct sensitivity experiments with the Community Atmosphere Model version 5 to understand the impact of representing heterogeneous distribution between cloud liquid and ice on the phase partitioning in mixed-phase clouds through different perturbations on the Wegener-Bergeron-Findeisen (WBF) process. In two experiments, perturbation factors that are based on assumptions of pocket structure and the partial homogeneous cloud volume derived from the High-performance Instrumented Airborne Platform for Environmental Research (HIAPER) Pole-to-Pole Observation (HIPPO) campaign are utilized. Alternately, a mass-weighted assumption is used in the calculation of WBF process to mimic the appearance of unsaturated area in mixed-phase clouds as the result of heterogeneous distribution. Model experiments are tested in both single column and weather forecast modes and evaluated against data from the U.S. Department of Energy (DOE) Atmospheric Radiation Measurement (ARM) Program's Mixed-Phase Arctic Cloud Experiment (M-PACE) field campaign and long-term ground-based multisensor measurements. Model results indicate that perturbations on the WBF process can significantly modify simulated microphysical properties of Arctic mixed-phase clouds. The improvement of simulated cloud water phase partitioning tends to be linearly proportional to the perturbation magnitude that is applied in the three different sensitivity experiments. Cloud macrophysical properties such as cloud fraction and frequency of occurrence of low-level mixed-phase clouds are less sensitive to the perturbation magnitude than cloud microphysical properties. Moreover, this study indicates that heterogeneous distribution between cloud hydrometeors should be treated consistently for all cloud microphysical processes. The model vertical resolution is also important for liquid water maintenance in mixed-phase clouds.

Key Points:
- Modeled mixed-phase cloud microphysical properties are sensitive to the perturbation of WBF process
- The heterogeneous spatial distribution between cloud hydrometeors should be consistently reflected in all microphysical parameterizations
- A physically based representation of heterogeneous structure will help to improve the phase partitioning of the Arctic mixed-phase clouds

Supporting Information:
- Supporting Information S1

Correspondence to:
X. Liu,
xliu6@uwyo.edu

Citation:
Zhang, M., Liu, X., Diao, M., D'Alessandro, J. J., Wang, Y., Wu, C., et al (2019). Impacts of representing heterogeneous distribution of cloud liquid and Ice on phase partitioning of Arctic mixed-phase clouds. *Journal of Geophysical Research: Atmospheres*, *124*, 13,071–13,090. https://doi.org/10.1029/2019JD030502

Received 19 FEB 2019
Accepted 12 NOV 2019
Accepted article online 18 NOV 2019
Published online 4 DEC 2019

1. Introduction

Surface air temperature in the Arctic has risen twice as fast as the global mean (Fyfe et al., 2013; Hartmann et al., 2013; Huang et al., 2017; Pithan & Mauritsen, 2014; Screen & Simmonds, 2010). Mixed-phase clouds, composed of a mixture of supercooled liquid droplets and ice crystals, are considered to play an important role in the Arctic climate change (Bennartz et al., 2013; Garrett & Zhao, 2006; Hofer et al., 2019). Observations indicate that mixed-phase clouds are ubiquitous in the Arctic throughout the years (de Boer et al., 2009; Shupe, 2011; Shupe et al., 2006). Single-layer stratiform mixed-phase clouds are frequently observed to comprise a liquid layer at the cloud top, from which cloud ice particles are continuously formed and precipitating out. The complex interactions between cloud microphysics, cloud top radiative cooling, turbulent mixing, and surface coupling enable this type of Arctic mixed-phase clouds to persist from a couple of hours to several days in the high latitudes (Morrison et al., 2012).

Because of the significant difference in radiative properties of liquid droplets and ice particles, the phase partitioning between cloud liquid and ice in mixed-phase clouds has considerable impacts on the surface energy budget and regional and global climate. The simulation of phase partitioning of mixed-phase

clouds is therefore of substantial importance for global climate models (GCMs) to have an accurate projection of the future climate change. However, considerable uncertainties are generally identified in GCMs in simulated partitioning between condensed cloud water content. For example, the supercooled liquid fraction (SLF), defined as the ratio of cloud liquid water path (LWP) over cloud total water path (TWP) (i.e., summation of LWP and ice water path (IWP)), exhibits large variabilities as a function of temperature in simulated mixed-phase clouds among GCMs that participate in the Coupled Model Intercomparison Project Phase 5 (CMIP5). The temperature at which supercooled liquid and ice are equally abundant differs by nearly 40°C in mixed-phase clouds over the Southern Ocean (McCoy et al., 2015, 2016).

One source for cloud phase biases that has not been fully understood lies in the discrepancy between number concentrations of ambient ice nucleating particles (INPs) and observed cloud ice particles. As mixed-phase cloud microphysical properties are largely sensitive to the cloud ice number concentration, either the bias in the representation of INPs (Fridlind et al., 2012; Xie et al., 2013) or the bias in the representation of secondary ice particle production (Field et al., 2017) may lead to errors in the modeled LWP and IWP. Earlier studies have found that reducing the overestimated INP number concentration can result in a substantial improvement in modeled LWP through a slowed-down Wegener-Bergeron-Findeisen (WBF) process (Liu et al., 2011; Xie et al., 2008).

The representation of WBF process, by which ice particles grow at the expense of coexisting cloud liquid due to the lower equilibrium water vapor pressure with respect to ice than liquid at subfreezing temperatures, also contributes to the large model biases in simulating mixed-phase clouds (Barrett et al., 2017a; Xie et al., 2008). Observations and numerical studies have illustrated that the strength of WBF process can be strongly influenced by the available supersaturation, which depends on the cloud dynamics (Fan et al., 2011; Korolev, 2007, 2008). For example, it is found that the growth of cloud ice particles at the expense of liquid droplets only takes place in ~50% of cloud volumes, predominantly in downdrafts when local water vapor pressure exceeds the saturation vapor pressure with respect to ice but remains lower than the saturation vapor pressure with respect to liquid (Fan et al., 2011). Strong updrafts, which provide excessive vapor pressure than the saturated vapor pressure with respect to both liquid and ice, allow ice particles and liquid droplets to grow simultaneously (Korolev, 2007, 2008; Korolev & Field, 2008). However, in strong downdrafts (mostly associated with deep convections) or near cloud boundaries where the ambient vapor pressure is no longer saturated with respect to ice, simultaneous evaporation of liquid droplets and ice crystals can occur.

The distribution of supercooled liquid droplets and ice particles inside mixed-phase clouds is also critical for the WBF process (Korolev et al., 2003; Korolev & Isaac, 2006). In situ measurements suggest that mixed-phase clouds may not consist of homogeneous distribution of liquid and ice, and pure liquid or pure ice pockets on the scales of 10^2 to 10^3 m are likely to exist (D'Alessandro et al., 2019; Korolev et al., 2003, 2017; Korolev & Isaac, 2006). Cloud volume that is saturated with respect to liquid is therefore largely reduced as the result of pure ice areas. The distribution of relative humidity with respect to liquid (RH) is then skewed toward a lower value below 100% (Fu & Hollars, 2004; Korolev & Isaac, 2006). Moreover, the heterogeneous distribution between liquid droplets and ice crystals also reduces the contact volume where ice crystals interact with liquid droplets. The volume that ice crystals grow at the expense of liquid water via the WBF process is therefore restricted (Tan & Storelvmo, 2016). The slowed-down WBF process will change the cloud phase and glaciation of mixed-phase clouds, which may ultimately affect the climate sensitivity estimated from GCMs (Tan et al., 2016).

The large discrepancies in phase partitioning of condensed cloud water between model simulations and observations can be largely addressed by improving the treatment of WBF process in GCMs. For example, by considering the impact of subgrid variability of in-cloud updrafts on the activation of WBF process, Storelvmo et al. (2008) found that the onset frequency of WBF process is significantly altered in mixed-phase clouds, yielding a smoother transition from liquid to ice that is more comparable to the observation. Furthermore, supercooled liquid droplets and ice crystals are generally assumed to homogeneously distribute inside mixed-phase clouds in each GCM grid cell. As a result, all condensed liquid water has the potential to be consumed by ice particles through the WBF process, particularly within a long model time step (20–30 min). Tan and Storelvmo (2016) pointed out that the heterogeneous distribution of liquid and ice in mixed-phase clouds can substantially extend the WBF process time scale by orders of magnitude because of the shrink of contact volume between the two phases.

The goal of this study is to understand the sensitivity of simulated Arctic mixed-phase clouds to the heterogeneous distribution of supercooled liquid droplets and ice particles in GCMs and how the change in WBF process would interact with other cloud microphysical processes. We test three different assumptions that mimic the consequences of heterogeneous distribution in mixed-phase clouds through perturbations on the WBF process with the Community Atmosphere Model version 5 (CAM5). Sensitivity experiments using the single column version of CAM5 are tested against extensive observations at the U.S. Department of Energy (DOE) Atmospheric Radiation Measurement (ARM) North Slope of Alaska (NSA) site during the Mixed-Phase Arctic Cloud Experiment (M-PACE) field campaign. Model experiments run in the weather forecast mode are compared with the long-term ground-based remote sensing data to understand the impact of perturbation on the seasonal variations of Arctic mixed-phase clouds.

The structure of this paper is organized as follows. The introduction of CAM5 model and sensitivity experiments are presented in section 2. Section 3 introduces the model approach including single column and global weather forecast modes. Section 4 presents the model results from single column simulations, and results from global simulations are provided in section 5. Summary and conclusions are given in section 6.

2. Model and Experiments

2.1. CAM5

The released CAM version 5.3 is used in this study (Neale et al., 2010). A two-moment cloud microphysical scheme (Morrison & Gettelman, 2008, hereafter as MG08) is included in CAM5, which parameterizes the microphysical processes of cloud hydrometeors of cloud liquid, cloud ice, rain, and snow. The mass mixing ratios and number concentrations of cloud liquid and cloud ice are prognostically calculated, while those of rain and snow are diagnosed. Other physical parameterizations in CAM5 include the three-mode version of modal aerosol module (MAM3) (Liu et al., 2012), Zhang and McFarlane (1995) deep convection parameterization, Park and Bretherton (2009) shallow convection scheme, and Bretherton and Park (2009) scheme for the planetary boundary layer (PBL) turbulence process. The Rapid Radiative Transfer Model for GCMs (RRTMG) (Iacono et al., 2008) is applied in the aerosol and cloud radiative transfer calculations.

As the default heterogeneous ice nucleation parameterization in CAM5, the Meyers et al. (1992) scheme was found to overestimate the nucleated ice number concentration in mixed-phase clouds (DeMott et al., 2010, 2015; Prenni et al., 2007). Different from the deterministic Meyers et al. parameterization, classical nucleation theory (CNT) follows the stochastic hypothesis that represents ice nucleation as a function of time (Chen et al., 2008; Hoose et al., 2010). The CNT scheme relates the heterogeneous ice nucleation rate to the properties of aerosol particles such as number concentrations and sizes of aerosol particles. By considering the heterogeneity in nucleation ability of individual aerosol particles, Wang et al. (2014) introduced a log-normal probability density function (PDF)-based treatment in contact angle to better represent the ice nucleation behavior. By replacing Meyers et al. ice nucleation scheme with CNT, Wang et al. (2018) showed that CAM5-simulated mixed-phase cloud phase partitioning in polar regions is significantly improved especially at temperatures colder than $-20°C$. In this study, the Meyers et al. scheme in the default CAM5 is replaced by CNT, and the model experiment is denoted as CTL (Table 1).

2.2. Treatment of WBF Process in Default CAM5

In the MG08 cloud microphysical scheme, when liquid and ice coexist at temperatures below $0°C$, the local (in-cloud) depositional growth rate A of cloud ice through the WBF process is given by

$$A = \frac{q_v^* - q_{vi}^*}{\Gamma_p \tau_i} \tag{1}$$

where q_v^* is the in-cloud water vapor mass mixing ratio at liquid saturation, q_{vi}^* is the in-cloud water vapor mass mixing ratio at ice saturation, and $\Gamma_p = 1+(L_s/c_p)(dq_{vi}/dT)$ is the psychrometric correction to account for the release of latent heat, in which L_s is the latent heat of sublimation, c_p is the specific heat at constant pressure, and (dq_{vi}/dT) is the change of ice saturation vapor pressure with temperature. q_v^* and q_{vi}^* are calculated according to the saturation vapor presssure with respect to liquid and ice, respectively. τ_i is the supersaturation relaxation time scale associated with ice deposition through the WBF process and is given by

Table 1
Model Experiments in M-PACE Case Study and Global Simulations

Experiments	Simulation type	Model description
CTL	SCM/nudging	Default model configuration but with CNT ice nucleation scheme. Nudging U, V (horizontal winds), and T (temperature) to the ERA-Interim reanalysis data when running the nudging simulation
WBF_TS16	SCM/nudging	Apply a constant perturbation value of 10^6 to the WBF process supersaturation relaxation time scale. Assume pockets with 100 m size uniformly distributed in grid cells as proposed by Tan and Storelvmo (2016)
WBF_HIPPO	SCM/nudging	Apply a constant perturbation value of 0.15 to the WBF process. Assume mixed-phase region occupies 15% fractional volume of mixed-phase clouds. Derived from HIPPO campaign
WBF_MSWT	SCM/nudging	Replace liquid saturated water vapor mixing ratio with mass-weighted water vapor mixing ratio in the WBF process calculation, following Fu and Hollars (2004)
WBF_TS16_ACC	SCM	Same as the WBF_TS16 but the constant perturbation factor is also applied to accretion of liquid droplets and rain drops by snow. Heterogeneous distribution is consistently considered in cloud microphysics
WBF_TS16_ACC_L60	SCM	Same as the WBF_TS16_ACC but utilizes 60 vertical layers
WBF_TS16_ACC_L120	SCM	Same as the WBF_TS16_ACC but utilizes 120 vertical layers

Note that sensitivity experiments share the same model configuration as CTL except for the designed modifications for sensitivity tests.

$$\tau_i = \left(2\pi N_{0i}\rho_\alpha D_v \lambda_i^{-2}\right)^{-1} \tag{2}$$

where D_v is the diffusivity of water vapor in air and N_{0i} and λ_i are the intercept and slope of the ice particle size distribution, respectively, represented by the gamma function (Morrison & Gettelman, 2008). Note that as the condensation and evaporation of cloud liquid water are not explicitly calculated in the MG08 microphysics, WBF process here directly converts available cloud liquid water to cloud ice and snow, rather than consuming the water vapor from liquid evaporation. Under the circumstances when liquid water is totally consumed in one model time step due to the WBF process, ice particles will continue to gain mass from water vapor through the depositional growth during the rest of that time step. Therefore, in terms of ice depositional growth in MG08, it is composed of two separate microphysical processes: one is the WBF process, by which cloud ice and snow grow at the expense of liquid water, and the other is ice depositional growth at the expense of water vapor. In the following discussion, we will refer the WBF to the first process whereas the latter process as the ice deposition. In addition to the CTL experiment with the above WBF treatment, three sensitivity experiments with modifications to the WBF process are conducted and will be discussed in the following subsections.

2.3. New WBF Treatment Based on Tan and Storelvmo (2016)

The WBF process largely depends on the contact volume between supercooled liquid droplets and ice crystals. The MG08 microphysics parameterization assumes that supercooled liquid droplets and ice crystals are homogeneously mixed within an individual grid box, and the contact volume between liquid and ice in a typical GCM grid box is on a magnitude of $O(10^3)$ m (vertically) $\times$ $O(10^5)$ m (horizontally) $\times$ $O(10^5)$ m (horizontally) = $O(10^{13})$ m^3. On the other hand, as noted in Tan and Storelvmo (2016), when pockets of pure liquid and pure ice with size of 100 m are assumed as they uniformly distribute on all sides in an alternating sequence, the contact volume between liquid and ice would be $O(10)$ m (vertically) $\times$ $O(10^3)$ m (horizontally) $\times$ $O(10^3)$ m (horizontally) = $O(10^7)$ m^3. The contact volume is reduced by six orders of magnitude compared to the homogeneous distribution. Such a difference in contact volume can be reflected in the WBF process rate because the WBF process is assumed to be inversely proportional to the supersaturation relaxation time scale τ_i (equation (1)), which is further inversely proportional to the contact volume. The WBF process rate is thus reduced by six orders of magnitude due to the heterogeneous structure of liquid and ice pockets in mixed-phase clouds. In this study, a sensitivity experiment using the perturbation to the WBF process following Tan and Storelvmo (2016) is conducted and denoted as WBF_TS16 (Table 1).

2.4. New WBF Treatment Based on HIPPO Data Analysis

The High-performance Instrumented Airborne Platform for Environmental Research (HIAPER) Pole-to-Pole Observation (HIPPO) Global campaign was operated by the Earth Observing Laboratory (EOL) of the National Center for Atmospheric Research (NCAR) during 2009 to 2011 (Wofsy et al., 2011). Five pole-to-pole research flight deployments (HIPPO#1-5) were conducted in total, and each campaign

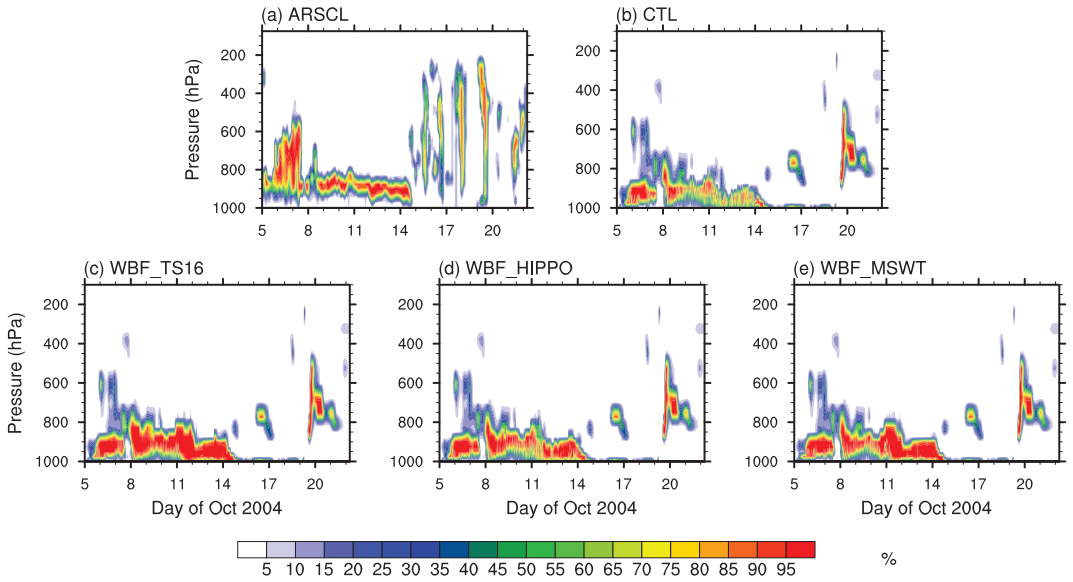

Figure 1. Time-pressure cross sections of modeled and observed cloud fraction at the Barrow site during the M-PACE filed campaign. (a) Observed frequency of occurrence of clouds from the Active Remotely Sensed Cloud Locations (ARSCL) algorithm. (b–e) SCM simulations. CTL is the default experiment assuming the homogeneous distribution; WBF_TS16 is the experiment with constant WBF perturbation scale of 10^6; WBF_HIPPO is the experiment assuming 15% volume of mixed-phase clouds are homogeneously mixed regions where a perturbation of 0.15 is applied to WBF process; WBF_MSWT is the experiment using mass-weighted water vapor mixing ratio treatment in the WBF process calculation.

included two flights over the Arctic from 60°N to 87°N and 135°W to 165°W. In this study, we utilize the raw 1 Hz in situ data of temperature and mass concentration, number concentration, and size distributions of cloud particles collected in the Arctic regions during HIPPO#2-5 to sample the heterogeneous structures of mixed-phase clouds, where the spatial resolution is 100–200 m depending on the aircraft speed. There are ~65 hr of total measurements during the analyzed time period, which corresponds to ~46,800 km of the flight track at the speed of 200 m/s.

Temperature was measured by the Rosemount temperature probe, with the accuracy and precision of 0.5 and 0.01 K, respectively. We focus on the temperature range between −40 and 0°C to exclude warm clouds and cirrus clouds. Cloud particles were measured by the cloud droplet probe (CDP) and fast two-dimensional cloud probe (2-DC). The CDP detects the number concentration of particles ranging from 2 to 50 μm, and the 2-DC measures the particles from 62.5 to 1600 μm. Particles with the size between 1600 and 3200 μm can be mathematically reconstructed. The mass concentrations from 2-DC are derived based on Brown and Francis (1995). Following the method of D'Alessandro et al. (2019), we define in-cloud conditions as when at least one of the two conditions is satisfied: (1) the CDP measured number concentration > 0.03 cm^{-3} and mass concentration $> 3.98\times10^{-4}$ g m^{-3}; (2) at least one particle is detected by the 2-DC, and its derived mass concentration is greater than 4.68×10^{-5} g m^{-3}. To further determine the cloud phase, we utilize the approach shown in Figure 1 of D'Alessandro et al. (2019) to categorize the detected particles into cloud liquid droplets and ice crystals and define cloud phase based on the mass fraction of LWC with respect to TWC. Following Korolev et al. (2003), clouds are considered as liquid phase when LWC/TWC ≥ 0.9, mixed phase when $0.1 <$ LWC/TWC < 0.9, and ice phase when LWC/TWC ≤ 0.1. We note that a "moving average" is conducted on the 1 Hz observation data to derive the 10 and 100 s averaged data, corresponding to 2 and 20 km spatial resolutions, to examine the impact of spatial scale on the inspected mixed-phase cloud structures.

Cloud phase determination in the HIPPO campaign is categorized into four temperature bins: −10–0°C, −20–−10°C, −30–−20°C, and −40–−30°C. The total flight time at each temperature bin and the probability of occurrence of each cloud phase at different temperature bins are listed in Table 2. Note that the cloud data discussed in the subsequent phase determination analysis are further sampled using a threshold of TWC ≥ 0.01 g m^{-3}, which is the main reason for more in-cloud samples at coarser scales. As shown in

Table 2
Number of Samples and Occurrence Frequency of Three Cloud Phases at Four Temperature Bins from 0 to −40°C in the HIPPO Global Campaign

Dataset	Temperature	Liquid phase (#)	Mixed phase (#)	Ice phase (#)	In-cloud (#)
Obs 1 s	-10°C ≤ T < 0°C	3115 (38.0%)	1953 (23.8%)	3134 (38.2%)	8202
	-20°C ≤ T < -10°C	784 (18.4%)	138 (3.2%)	3328 (78.3%)	4250
	-30°C ≤ T < -20°C	263 (7.2%)	178 (4.9%)	3209 (88.0%)	3650
	-40°C ≤ T < -30°C	3 (0.3%)	10 (1.0%)	919 (98.6%)	932
	Total	4165 (24.5%)	2279 (13.4%)	10590 (62.2%)	17034
Obs 10s	-10°C ≤ T < 0°C	3373 (38.0%)	2562 (28.8%)	2949 (33.2%)	8884
	-20°C ≤ T < -10°C	834 (19.5%)	206 (4.8%)	3237 (75.7%)	4277
	-30°C ≤ T < -20°C	242 (6.9%)	271 (7.7%)	3007 (85.4%)	3520
	-40°C ≤ T < -30°C	0 (0.0%)	13 (1.4%)	898 (98.6%)	911
	Total	4449 (25.3%)	3052 (17.3%)	10091 (57.4%)	17592
Obs 100 s	-10°C ≤ T < 0°C	4715 (40.4%)	4570 (39.2%)	2388 (20.5%)	11673
	-20°C ≤ T < -10°C	1125 (22.7%)	492 (9.9%)	3337 (67.4%)	4954
	-30°C ≤ T < -20°C	280 (6.7%)	520 (12.4%)	3385 (80.9%)	4185
	-40°C ≤ T < -30°C	0 (0%)	29 (3.2%)	883 (96.8%)	912
	Total	6120 (28.2%)	5611 (25.8%)	9993 (46.0%)	21724

Table 2, the occurrence frequency of mixed phase portions increases as temperature warms. Under all three spatial resolutions, clouds with coexisting liquid and ice occur with the highest frequency in the temperature bin of −10–0°C. The temperature bin between −30 and −20°C shows the second highest frequency of mixed phase area. In general, mixed phase area in the temperature range of −40–0°C only occupies ~13.4% of total clouds based on 1 Hz data. The occurrence frequency of mixed-phase regions tends to increase when the averaging scale expands. Table 2 demonstrates that the homogeneously mixed-phase region should not always exist but is more likely to occupy limited cloud volumes in the temperature range of −40–0°C.

We therefore propose that liquid and ice homogeneously mixed regions only have ~15% fractional volume of the clouds in the temperature range between −40 and 0°C. We note that this 15% is likely an underestimation of the homogeneously mixed regions inside mixed-phase clouds, because pure liquid clouds or pure ice clouds may be sampled as mixed-phase clouds in our sampling strategy. Moreover, we note that the aircraft observations are inherently based on the 1-D measurements, which is not exactly a sampling of the 3-D volume in a GCM grid box. However, the 15% estimate made here is based on a statistical distribution of cloud segments from 21,724 aircraft samples on 20 km scales, which should be statistically representative of a 3-D volume. Additionally, the sampling approach in the HIPPO campaign has no preference for inside or outside of clouds; thus such a statistical analysis is not biased toward one type of clouds or a certain level in a cloud. As the WBF process only occurs in the homogeneously mixed regions, the limited mixed-phase volume will cause a lower WBF process rate. As noted in the earlier section, since the WBF process rate is proportional to the mixed volume, a perturbation factor of 0.15 is applied to equation (1) to represent the 15% of homogeneously mixed regions. The model experiment with WBF process activated at only 15% of the grid cell is referred to as WBF_HIPPO in the following discussion.

2.5. New WBF Treatment Based on Mass-Weighted Water Vapor

Earlier theoretical studies and in situ measurements elucidated that RH is close to 100% in mixed-phase clouds with the temperature range between −35 (generally above −30°*C*) and −5°*C* due to the fact that liquid droplet evaporation is much faster than ice deposition (D'Alessandro et al., 2019; Korolev & Isaac, 2006; Korolev & Mazin, 2003). Conversely, Fu and Hollars (2004) argued that the scenario that RH remains saturated with respect to liquid could be true only when liquid droplets and ice crystals are homogeneously mixed in space. They found that RH in observed Arctic mixed-phase clouds substantially deviated from the saturation water vapor with respect to liquid. They hypothesized that the possible heterogeneous distribution between cloud particles on the scale of 100 m may explain the discrepancy in observed RH inside mixed-phase clouds. In addition, Fu and Hollars (2004) found that a mass-weighted representation of RH can better represent the observed RH values in the Arctic mixed-phase clouds, which may reflect the consequence of heterogeneous distribution.

In MG08 cloud microphysics, the homogeneous distribution between liquid and ice is assumed, and the WBF process rate is determined based on the difference between saturated water vapor mixing ratio

with respect to liquid and saturated water vapor mixing ratio with respect to ice. However, according to Fu and Hollars (2004), such an assumption of water vapor mixing ratio at liquid saturation may not be valid when heterogeneous distribution of condensed cloud water exists in mixed-phase clouds. To take the heterogeneous distribution into account, a mass-weighted water vapor mixing ratio is used to replace the saturated water vapor mixing ratio with respect to liquid in the WBF process calculation (equation (1)).

$$q_v = q_{vl} \times \frac{LWC}{TWC} + q_{vi} \times \frac{IWC}{TWC} \tag{3}$$

where q_{vl} is the water vapor mixing ratio at liquid saturation and q_{vi} is the water vapor mixing ratio at ice saturation. LWC and IWC are total in-cloud liquid water mass mixing ratio (liquid + rain) and total in-cloud ice water mass mixing ratio (ice + snow), respectively, and total water content (TWC) is sum of LWC and IWC. As the rate of WBF process and ice depositional growth is now related to the mass partitioning of condensed cloud water, the impact of heterogeneous distribution such as pure liquid or pure ice on the WBF process can be represented in this mass-weighted treatment (MSWT). For example, when pure ice exists in the mixed-phase cloud, q_v in equation (3) should be q_{vi} as LWC equals to 0. The difference between q_v and q_{vi} in equation (1) will then become 0, and the WBF process effectively shuts down. A varying condition between homogeneous distribution and heterogeneous distribution is represented, as q_v changes between q_{vl} and q_{vi} depending on the partitioning of condensed cloud water. Note that the mass-weighted assumption has been used before without using heterogeneous distribution of cloud liquid and ice in mixed-phase clouds as the justification for the assumption (Lord et al., 1984; Wood & Field, 2000). Therefore, this assumption is indirectly related to the existence of heterogeneity of mixed-phase clouds. We denote this sensitivity experiment as WBF_MSWT in the following discussion.

3. Model Approach

3.1. Single Column Modeling

Single column model (SCM) has been widely used in developing and testing physics parameterizations in GCMs (Klein et al., 2009; Liu et al., 2007, 2011; Morrison et al., 2009; Xie et al., 2005; Yuan et al., 2006). With large-scale circulation forced by observations, SCM results can be directly compared to observational data to evaluate the model behavior due to the change in physical parameterizations. The CAM5 SCM utilized in this study is run under the Eulerian dynamic core with 30 vertical layers and 20-min time step. The physics parameterizations in SCM are the same as standard CAM5. SCM experiments are run for the period of M-PACE field campaign which was conducted at the ARM NSA Barrow site in October 2004 (Verlinde et al., 2007). To constrain SCM for the M-PACE field campaign, large-scale forcings including advections and divergences of temperature (T) and moisture (Q), and surface fluxes are derived following Xie et al. (2006). In order to provide a reasonable aerosol field for the SCM simulation of Arctic mixed-phase clouds, aerosol size distribution and number mixing ratios are prescribed with the in situ data following Liu et al. (2011). Sulfate, primary organic matter (POM), sea salt, and mineral dust are categorized in the corresponding MAM modes. The mass fraction for each aerosol species in each mode is prescribed as 70% POM and 30% sulfate in the accumulation mode and 85% sea salt, 10% sulfate, and 5% mineral dust in the coarse mode. Number concentrations of cloud droplets and ice crystals are then calculated online by the cloud microphysics in SCM.

3.2. Global Modeling

CAM5 is also run in the global mode using 1.9° ×2.5° horizontal resolution and 30 vertical levels with 8 levels below 2 km. The nudging technique is utilized in global simulations to constrain simulated horizontal wind (U, V) and temperature (T) fields toward the ERA-Interim reanalysis data from the European Center for Medium-Range Weather Forecasts (ECMWF). Three-year simulations are run from November 2005 to December 2008 to examine the impact of perturbation to the WBF process treatment on seasonal variations of modeled mixed-phase cloud properties. The first 2-month results are used as model spin-up, whereas the rest of the simulations are for model analysis. Model results are 3 hourly outputted to sample low-level stratiform mixed-phase clouds. We select the land grid that is closest to the NSA Barrow site (located at 71.3°N, 156.6°W) to evaluate low-level mixed-phase clouds against

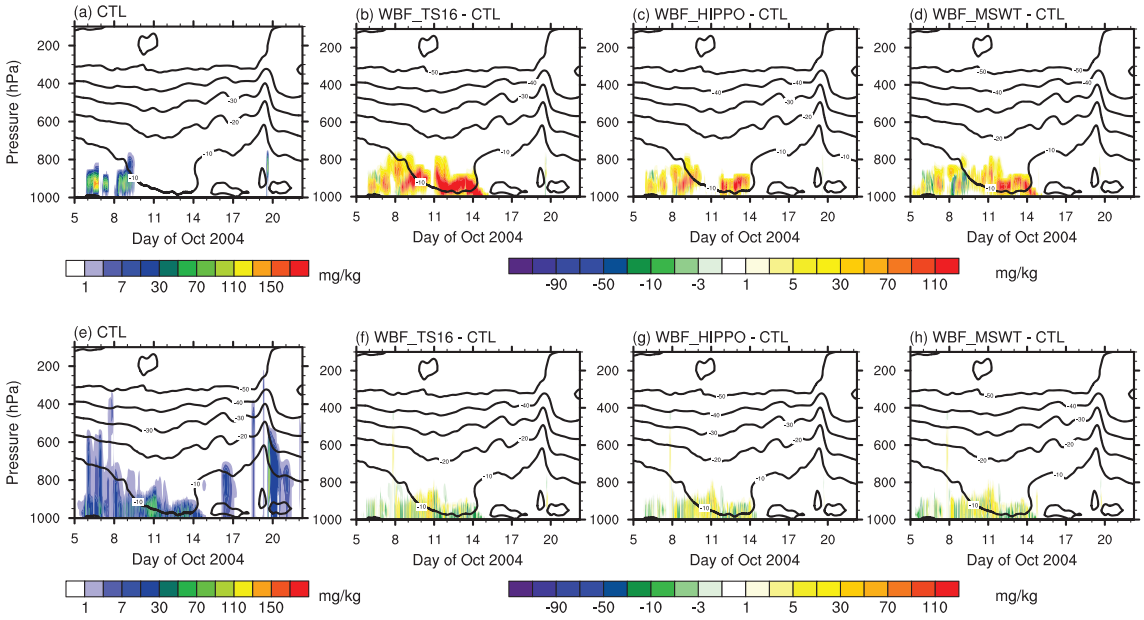

Figure 2. Time-pressure cross sections of modeled cloud liquid water (including rain; a–d) and cloud ice water (including snow; e–h) mass mixing ratios at the Barrow site during the M-PACE filed campaign from CTL and the difference between three sensitivity experiments (WBF_TS16, WBF_HIPPO, and WBF_MSWT; from left to right) and CTL. Black contours are the ambient temperatures.

the ARM ground-based; observational data. Model results using an ocean grid are not significantly different.

4. Single Column Model Results

4.1. Modeled Cloud Properties in M-PACE

Simulations of Arctic mixed-phase clouds from CAM5 SCM are evaluated against the ground-based observations in M-PACE. Figure 1 shows the comparison of time-pressure cross sections between observed frequency of cloud occurrence and SCM simulated cloud fraction in the CTL and three sensitivity experiments. The observed frequency of occurrence of clouds is derived from the Active Remotely Sensed Cloud Location (ARSCL) algorithm (Clothiaux et al., 2000), which provides the vertical location of clouds by integrating measurements of Millimeter Wave Cloud Radar, Micropulse Lidar (MPL), and laser ceilometers. The observation data were collected at 10-s and 45-m intervals and are now averaged into 3-hour and 25-hPa intervals so that it can be better compared with the clouds from model simulations. Figure 1a indicates that, at the NSA Barrow site, multilayer clouds were observed during 5–8 October and followed by continuous single-layer mixed-phase clouds between 8 and 14 October. Deep clouds associated with frontal systems dominated the last several days of M-PACE. In general, compared to observations, SCM poorly simulates the multilayer clouds at the beginning and the frontal systems in the later campaign period. Between 8 and 14 October, although temporal patterns of clouds are relatively well produced by CTL, the cloud fraction is largely underestimated, and the modeled cloud base is too low compared to observations. The bias in modeled cloud base can be explained by the overestimated specific humidity and RH near the surface (shown in Figure S1), which is probably due to the biased forcing of water vapor advection or surface fluxes that drive the SCM. Moreover, the underestimation of cloud fraction is likely attributed to cloud microphysics since condensed cloud water is mostly in ice phase in CTL (shown in Figure 2), and ice particles go through rapid growth at the expense of water vapor and reduce the ambient RH. Figures 1c–1e show the improvements in modeled cloud fraction in the three sensitivity tests with perturbed WBF treatments. Cloud fraction at layers between 950 hPa and 850 hPa increases substantially compared to CTL. We note that comparable improvements are found in WBF_TS16 and WBF_MSWT, while WBF_HIPPO shows a smaller increase of cloud fractions between 10 and 12 October than these two experiments. However, it should be noted that the corrections tend to over-simulate cloud fraction, and the cloud layers are significantly too deep. Cloud base and cloud top both remain too low compared to the observations.

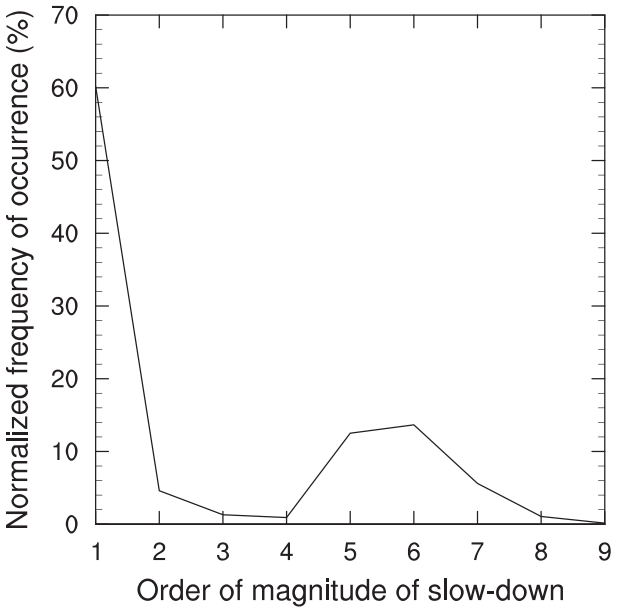

Figure 3. Frequency of occurrence of the slow-down magnitude on the WBF process as a result of using mass-weighted water vapor mixing ratio. The WBF process slow-down magnitude is calculated as the ratio of perturbed WBF process rate from the mass-weighted treatment over the WBF process rate that is calculated by the default treatment from 5 October to 22 October in SCM. The order of slow-down magnitude from 1–9 corresponds to a tuning factor between 10^{-1} and 10^{-9} in cloud microphysics.

Figure 2 shows the time-pressure cross sections of total LWC (sum of cloud liquid and rain) and total IWC (sum of cloud ice and snow) from CTL and the differences between CTL and the three perturbed simulations. It is shown in Figure 2a and 2e that CTL produces negligible LWC except for 6–9 October; and most of the condensed cloud water are partitioned into solid phase in which snow water dominates the total ice mass mixing ratio because of the fast autoconversion of cloud ice to snow (to be shown in Figure 6). The inconsistency between cloud microphysics for cloud water and macrophysics for cloud fraction is apparent in SCM CTL results when comparing modeled cloud fraction in Figure 1 and cloud water mass mixing ratios in Figure 2. The three sensitivity tests using different assumptions for the heterogeneous distribution between liquid and ice in mixed-phase clouds strongly increase LWC compared to CTL. We note that WBF_TS16 most substantially increases LWC in the low-level single-layer mixed-phase clouds during M-PACE. Using a much smaller magnitude of perturbation to the WBF process, WBF_HIPPO increases modeled LWC the least. The mass-weighted water vapor hypothesis in WBF_MSWT increases the LWC by the extent less than WBF_TS16 but more than WBF_HIPPO. Such a difference indicates that the perturbation to the WBF process in WBF_MSWT has an equivalent magnitude between 10^{-6} and 0.15, which implies that mass-weighted water vapor mixing ratio in equation (3) is able to describe an intermediate but varying condition between the extreme pocket structure proposed by Tan and Storelvmo (2016) and the partial homogeneous distribution found in our HIPPO data analysis. In Figure 3, we show the probability of occurrence of the slow-down magnitude when mass-weighted treatment is introduced to the WBF process. The slow-down magnitude is defined as the ratio of perturbed WBF process rate using the mass-weighted treatment over the default WBF process rate. It is demonstrated that the WBF process in WBF_MSWT is slowed down by factors spanning nine orders of magnitude (from 10^{-9} to 10^{-1}) depending on the partitioning of mixed-phase cloud water. One interesting finding is that the perturbation tends to peak around 10^{-1} and has another peak between 10^{-6} and 10^{-5}, which coincidentally correspond to the perturbations in WBF_HIPPO and WBF_TS16, respectively. The peak around 10^{-1} results from liquid dominant cloudy areas, while the peak between 10^{-6} and 10^{-5} is mostly associated with cloud ice-dominant areas (shown in Figure S2).

Total IWC from three sensitivity tests are shown in Figures 2f–2h. Compared to CTL, modeled IWC changes less than LWC when perturbing the WBF process. In addition, modeled IWC shows both increased and decreased patterns between 9 and 14 October in the low-level mixed-phase clouds. As the decrease of IWC is expected due to the slowing down of ice particle growth, the increase of both LWC and IWC implies that the total condensed cloud water amount has increased. Similar change is found in the IWC vertical profiles as shown in Figure 4, where IWC increases by 25%–50% in sensitivity experiments compared to CTL. The increased amount of total condensed water can probably be explained by the interaction between cloud microphysics and cloud top radiative cooling. As more cloud liquid water is simulated, cloud top radiative cooling can be enhanced to decrease the cloud top temperature (shown in Figure S1). Larger amount of water vapor therefore could be condensed in simulated low-level mixed-phase clouds.

Figure 4 compares the vertical profiles of total LWC and IWC with remote sensing retrievals based on Shupe et al. (2008). Both model and observations are averaged between 1200 UTC 9 October and 1200 UTC 10 October to obtain the vertical profiles in M-PACE. Despite the significant underestimation of LWC in CTL, the three sensitivity tests with perturbed WBF treatments still cannot produce comparable LWC to the observation. Even with the largest reduction in WBF process rate, WBF_TS16 still underestimates LWC by a factor of 2. Note that the peak of observed LWC is ~0.4 g m^{-3} at 1.2 km located in the upper cloud layers. However, simulated cloud layers tend to peak 0.6 km lower than observations, and cloud base is simulated only ~0.1 km above the surface in all the SCM experiments. As aforementioned, the too low cloud boundary is likely due to the bias in the forcing data that drive the SCM.

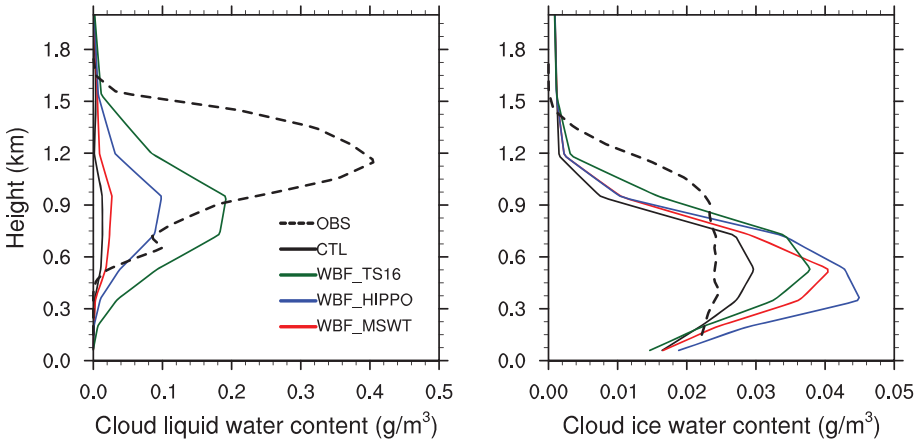

Figure 4. Vertical profiles of cloud liquid water content (left) and cloud ice water content (right), averaged between 1200 UTC 9 October and 1200 UTC 10 October during M-PACE. Black dash lines are retrieved liquid and ice water contents from Shupe et al. (2008). Solid black lines represent the SCM CTL. Solid green lines represent WBF_TS16, and solid blue lines are WBF_HIPPO. WBF_MSWT is shown with solid red lines.

Figure 5 shows the modeled LWP and IWP during the M-PACE, in which rain water and snow water mass mixing ratios are included in the integration of LWP and IWP. Observed LWP is retrieved from Wang (2007) based on the ARM Microwave Radiometer (MWR) measurements, while IWP is derived with the combined radar and lidar retrieval algorithm based on Millimeter Wave Cloud Radar and MPL measurements (Wang

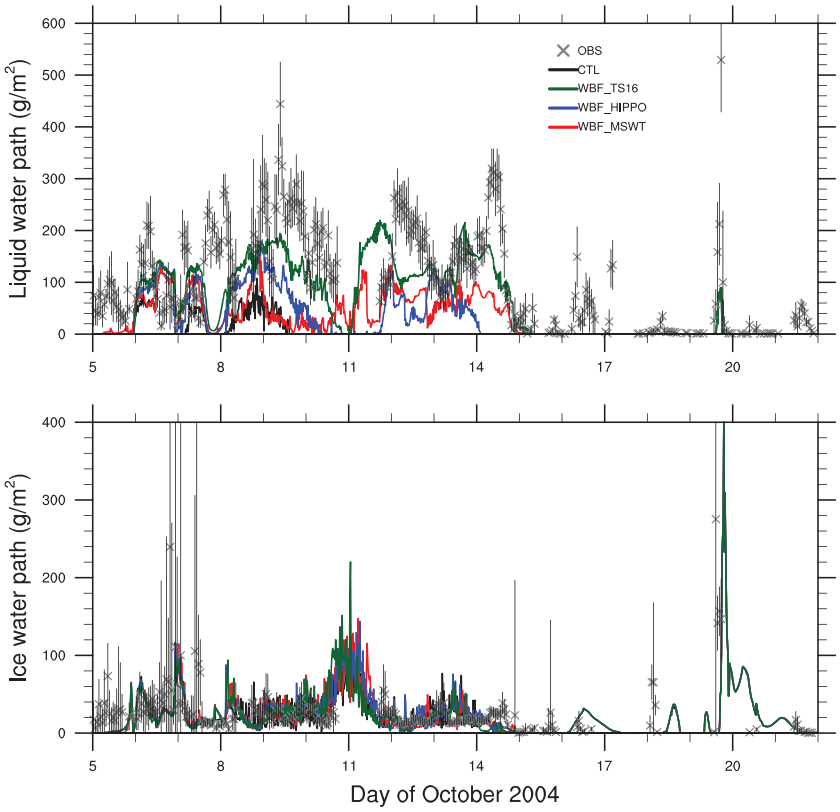

Figure 5. Liquid water path (upper panel) and ice water path (lower panel) from SCM simulations compared with the ground-based observation at the NSA Barrow site during the M-PACE campaign. Gray crosses represent observations from remote sensing retrievals including LWP from Wang (2007) and IWP from Wang and Sassen (2002). Gray straight lines on crosses indicate the one standard deviation of observed LWP and IWP. Solid black lines represent CTL simulation while solid green lines represent WBF_TS16, solid blue lines are WBF_HIPPO, and solid red lines are WBF_MSWT.

& Sassen, 2002). The mean bias in retrieved IWP is less than 35% (Khanal & Wang, 2015). As shown in Figure 5, the observed low-level mixed-phase clouds in the M-PACE field campaign are sustained with LWP larger than 100 g m^{-2} between 6 and 14 October. However, CTL only has a noticeable LWP before 10 October, and LWP is close to 0 for the remaining time period. The three sensitivity experiments improve not only the amount of LWP but also the maintenance of cloud liquid layers. The change in cloud LWP tends to depend on the perturbation magnitude in WBF process, as WBF_TS16 with the strongest perturbation produces the highest LWP and longest duration of LWP, and WBF_HIPPO has the lowest LWP since the magnitude of perturbation is nearly five orders of magnitude smaller. With a varying and intermediate perturbation magnitude between these two, WBF_MSWT has a comparable duration of cloud liquid water as WBF_TS16, but the increase of LWP is similar to WBF_HIPPO. Conversely, modeled IWP has a lower sensitivity to the WBF perturbation, which may result from the effect of other compensating cloud ice phase microphysical processes, such as accretion of snow. More discussion about the interaction of WBF process with other cloud microphysical processes will be presented in the next section.

4.2. Microphysics Processes

To understand how the perturbation of WBF process that follows the three different heterogeneity assumptions of mixed-phase clouds would affect the simulated cloud properties, budgets of process tendencies for cloud liquid, cloud ice, rain, and snow are examined in this section. Process tendencies are averaged between 9 and 13 October from SCM results. Figure 6 compares the process tendencies of cloud liquid water mass mixing ratio from cloud microphysics, as well as from cloud macrophysics, shallow convection, and PBL turbulence in the CTL and three sensitivity experiments. It is shown in Figure 6 that liquid water detrainment from shallow convection constitutes the majority of liquid source in mixed-phase clouds (i.e., 900–950 hPa) in CTL, while condensation by cloud macrophysics plays a secondary role and mainly contributes to liquid water formation near cloud top and bottom. Liquid water evaporation and several cloud microphysical processes consume the available cloud liquid. For example, conversions of liquid to ice and snow through the WBF process are important sink terms for the mass mixing ratio of liquid cloud water in CTL. With the strongest restriction in the WBF process, as shown in Figure 6b, WBF_TS16 nearly shuts down the WBF process, and instead the accretion of liquid by snow and vertical diffusion by PBL turbulence and shallow convection transport become more effective to consume liquid water. The increased liquid water sinks through vertical diffusion and shallow convection transport result from the interaction between cloud microphysics and other physical parameterizations. Nevertheless, detrainment of cloud liquid from shallow convection also becomes stronger, resulting in larger amounts of simulated LWC in WBF_TS16. In WBF_HIPPO and WBF_MSWT, although the tendency of WBF process indicates a small difference from CTL, other physical processes such as the cloud liquid water evaporation slow down. Detrainment from shallow convection is enhanced significantly in WBF_HIPPO, which leads to the increase of LWC. However, the accretion of liquid by snow water is increased in WBF_HIPPO and WBF_MSWT, compensating the slightly reduced cloud liquid sink through the WBF process. Note that the heterogeneous distribution between liquid and ice should also reduce the opportunity of liquid accretion by snow in mixed-phase clouds. The contrary increased tendency of accretion process indicates that the heterogeneous spatial distribution of cloud hydrometeors is not consistently reflected in all the cloud microphysical parameterizations. A sensitivity test will be conducted in section 4.3 to illustrate the effect of a consistent treatment in accretion process on simulated mixed-phase cloud properties. Note that modeled rain water mass mixing ratio is less sensitive to the WBF process perturbation in our sensitivity experiments (shown in Figure S3).

Figure 7 shows the budgets of process tendencies for cloud ice water from four SCM simulations. In general, CTL, WBF_HIPPO, and WBF_MSWT have three major sources for cloud ice mass mixing ratio, including WBF process at the expense of liquid water, ice depositional growth at the expense of water vapor, and the detrainment of cloud ice from shallow convection. The combined effect from WBF process and ice depositional growth explains the large underestimation of modeled cloud liquid water in CTL. As introduced in section 2.2, the WBF process and ice depositional growth at the expense of water vapor are two separate microphysical processes treated in MG08, in which the WBF process is calculated to consume available cloud liquid, whereas the ice depositional growth is determined for ice particles to continue their growth through a deposition of water vapor after all liquid water has been consumed. The strength of ice deposition can be used to infer whether cloud liquid water is completely or partially consumed in the model. It is

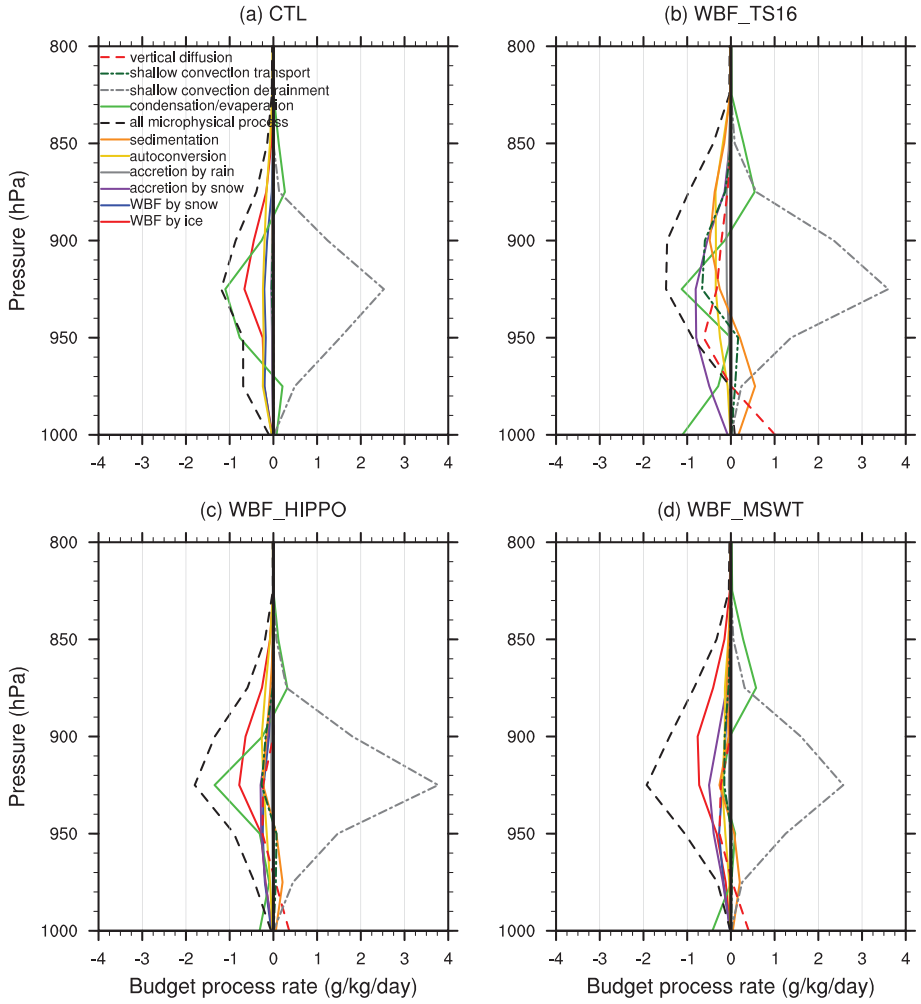

Figure 6. Process budget analysis associated with cloud liquid water tendencies from cloud microphysical processes, condensation/evaporation process from cloud macrophysics, and other physical processes from shallow convection and PBL turbulence schemes in SCM CTL and three sensitivity experiments. Process tendencies are averaged between 9 and 13 October 2004.

indicated in Figure 7b that the above two processes for cloud ice are completely inhibited in WBF_TS16. The strength of ice depositional growth is significantly reduced in WBF_HIPPO and WBF_MSWT compared to CTL (Figures 7c and 7d), which implies that the occurrence of partial depletion of liquid water is more frequent after perturbing the WBF process. Some of the formed cloud ice particles are depleted by sedimentation, while a larger fraction of cloud ice mass is removed by autoconversion to snow. Snow therefore dominates the solid phase in modeled mixed-phase clouds. Detrainment from shallow convection contributes to the snow water mass mixing ratio and induces the fast increase of snow mass through collection of liquid droplets and rain drops, where the process tendencies of collection of liquid and rain are much larger in WBF_TS16 than other experiments (Figure S4). Conclusively, the perturbation of WBF process plays an important role in reducing the probability of occurrence of complete consumption of the available cloud liquid water in the modeled mixed-phase clouds. Thus, the depositional growth of ice particles at the expense of water vapor is less frequently invoked, and the generation of snow water becomes less effective in the model.

4.3. Sensitivity Tests with Respect to Accretion and Model Vertical Resolution

As shown in the earlier discussion, when considering the heterogeneous distribution in mixed-phase clouds, a consistent treatment in all parameterizations is important for cloud microphysics. In this section, we investigate whether the consistent treatment would further improve the model performance of Arctic mixed-

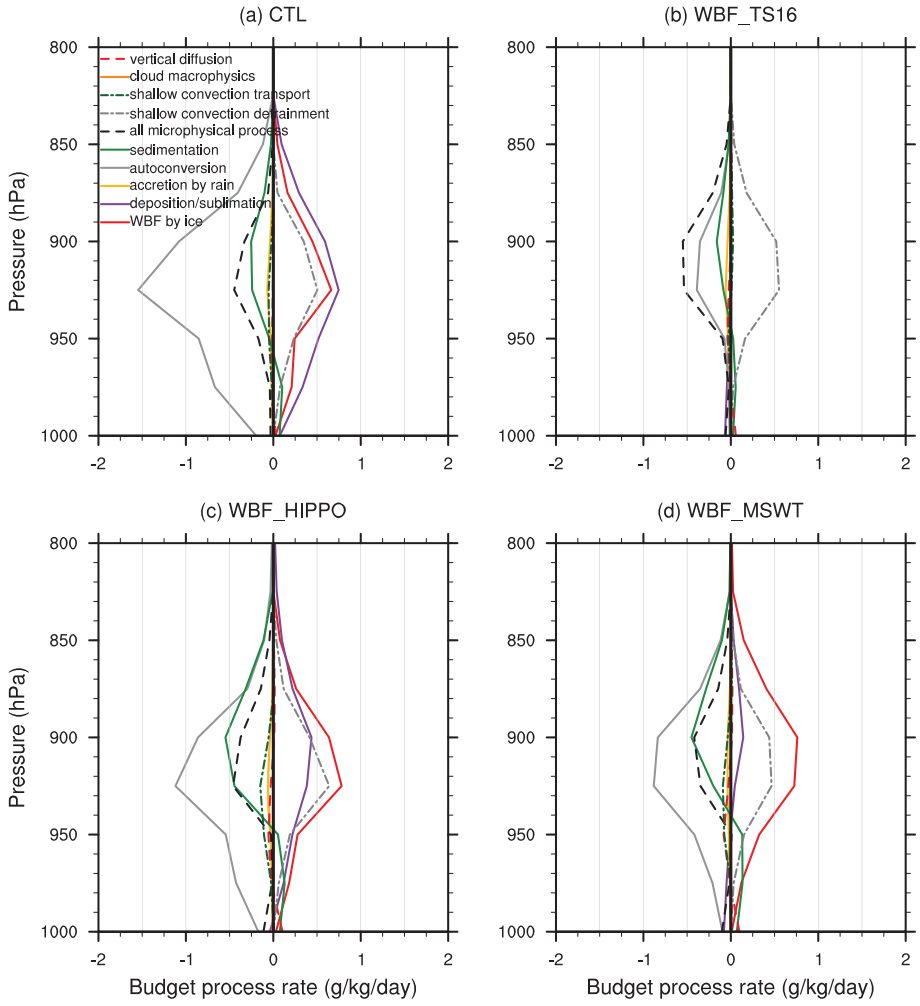

Figure 7. Same as Figure 6 but for cloud ice physical processes.

phase clouds. WBF_TS16 is utilized as an example to examine the model sensitivity to this change. Since WBF_TS16 is equivalent to slowing down the WBF process by having a factor of 10^{-6} on equation (1), to achieve our goal, a same perturbation parameter of 10^{-6} is applied to the calculation of accretion of liquid and rain by snow hydrometeor. This experiment is denoted as WBF_TS16_ACC (Table 1). Figure 8 shows the vertical profiles of modeled and observed cloud fraction, LWC, and IWC averaged between 1200 UTC 9 October and 1200 UTC 10 October during M-PACE. It is indicated that, although SCM still produces too low cloud boundaries compared to observations, LWC from WBF_TS16_ACC is much improved after a consistent treatment in cloud microphysics, compared to WBF_TS16. Moreover, the overestimation of IWC in WBF_TS16 is alleviated after the consistent treatment. However, the modeled IWC is now too low probably due to the coarse model vertical resolution.

Barrett et al. (2017b) revealed that the model vertical resolution is essential for the maintenance of cloud liquid layers in mixed-phase clouds. Therefore, we conduct two additional sensitivity experiments (WBF_TS16_ACC_L60 and WBF_TS16_ACC_L120 in Table 1), which are the same as the WBF_TS16_ACC, but with the model vertical layers increased from the default 30 layers to 60 and 120 layers, respectively. As shown in Figure 8, bias in the modeled cloud boundaries is not alleviated by increasing the model vertical resolution. However, the simulated mixed-phase clouds contain comparable amounts of cloud liquid and ice water as the observations. These results demonstrate that a consistent treatment in all cloud microphysical processes is important when considering the heterogeneous distribution of cloud hydrometeors. Meanwhile, the high vertical resolution also helps to improve the model behavior of Arctic mixed-phase clouds.

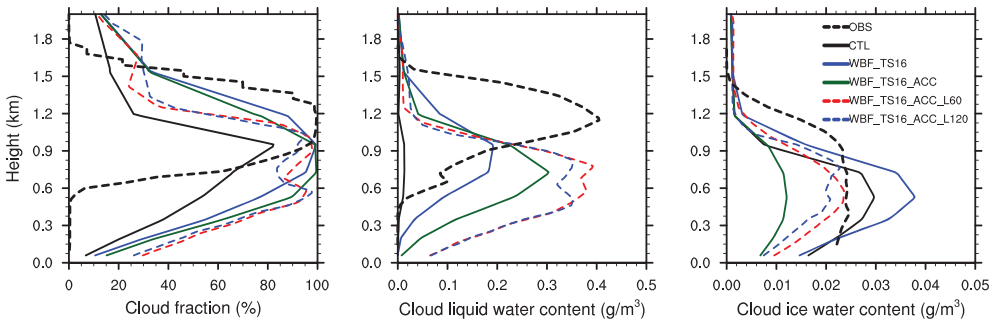

Figure 8. Vertical profiles of cloud fraction (left), cloud liquid water content (middle), and cloud ice water content (right) averaged between 1200 UTC 9 October and 1200 UTC 10 October during M-PACE. Cloud fraction observations are from ARSCL, and LWC and IWC profiles are retrieved by Shupe et al. (2008). Solid black lines represent the SCM CTL, solid blue lines for WBF_TS16, and solid green lines for WBF_TS16_ACC. Dashed lines are for sensitivity experiments with different vertical resolutions, as red for 60 vertical layers and blue for 120 vertical layers.

5. Global Model Results

In this section, we will discuss how the perturbation of WBF process impacts the seasonal variability of occurrence of low-level mixed-phase clouds and their microphysical properties in the Arctic.

5.1. Cloud Occurrence

To evaluate the model performance on frequency of cloud occurrence, 3-hourly model output of low-level mixed-phase clouds is sampled when (1) temperature is within 0 and $-40°C$; (2) the sum of cloud liquid water and rain water mass mixing ratios and the sum of cloud ice water and snow water mass mixing ratios are both greater than 0.001 g kg^{-1}; and (3) cloud top is below 700 hPa altitude. Similar sensitivity experiments as SCM (Table 1) are conducted but using the global model with horizontal wind and temperature fields nudged to ERA-Interim reanalysis. Model results from 2008 to 2010 are utilized for the analysis. The ground-based remote sensing observations were collected between 2013 and 2017 at the ARM NSA Barrow site (Zhang et al., 2014, 2019). We note that although there is a deviation in time between modeled and observed clouds, the 5-year statistics in observed cloud properties should not be expected to change significantly with time. Therefore, here we qualitatively examine the model response to the perturbation of the WBF process. Model outputs on the land grid that is closest to the Barrow site (71.3°N, 156.6°W) are used.

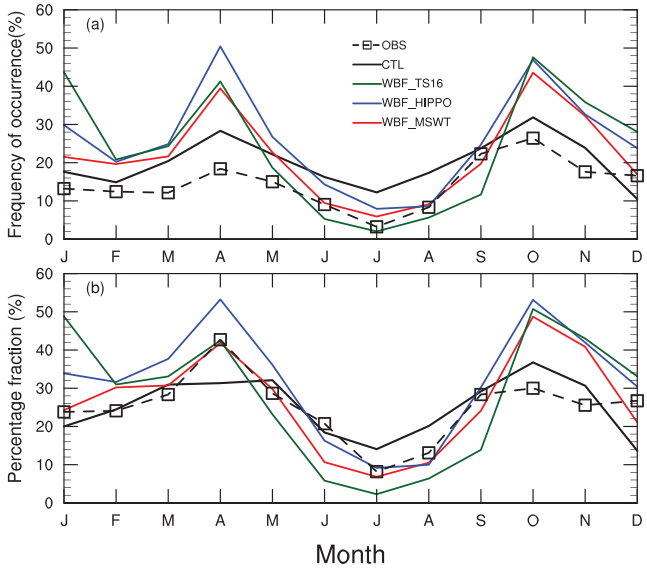

Figure 9. Comparison of (a) frequency of occurrence of observed single-layer stratiform mixed-phase clouds and modeled low-level mixed-phase clouds and (b) fractional percentage relative to all clouds at the NSA Barrow. Frequency of occurrence of mixed-phase clouds is the ratio of number of profiles of single-layer mixed-phase clouds over the number of all profiles including both cloudy and clear-sky profiles, while fractional percentage is the ratio over cloudy-sky profiles.

Figure 9 shows the comparison between monthly observed frequency of occurrence of single-layer stratiform mixed-phase clouds and modeled low-level mixed-phase clouds, as well as the percentage fraction of sampled mixed-phase clouds to all clouds. Frequency of occurrence is calculated as the ratio of single-layer stratiform mixed-phase cloud profiles to all-sky profiles, while the percentage fraction is determined as the ratio of single-layer stratiform mixed-phase cloud profiles to only cloudy-sky profiles. The observed single-layer mixed-phase clouds indicate significantly higher frequency of occurrence in spring and fall at Barrow. Compared to the observation, CTL generally produces the seasonality of observed frequency of occurrence of low-level mixed-phase clouds, but the frequency of occurrence is overestimated for all seasons, and the percentage fraction in spring is underestimated. Similarities in the change of model behavior are found in the three sensitivity experiments compared to CTL. For example, the peaks of frequency of occurrence in spring and fall are largely enhanced due to the slowed-down WBF process which helps to maintain more mixed-phase clouds. Meanwhile, the low frequency of occurrence in warm seasons is reduced with the WBF perturbation, which may be related to the higher cloud top as Figure 10 shows that the cloud top

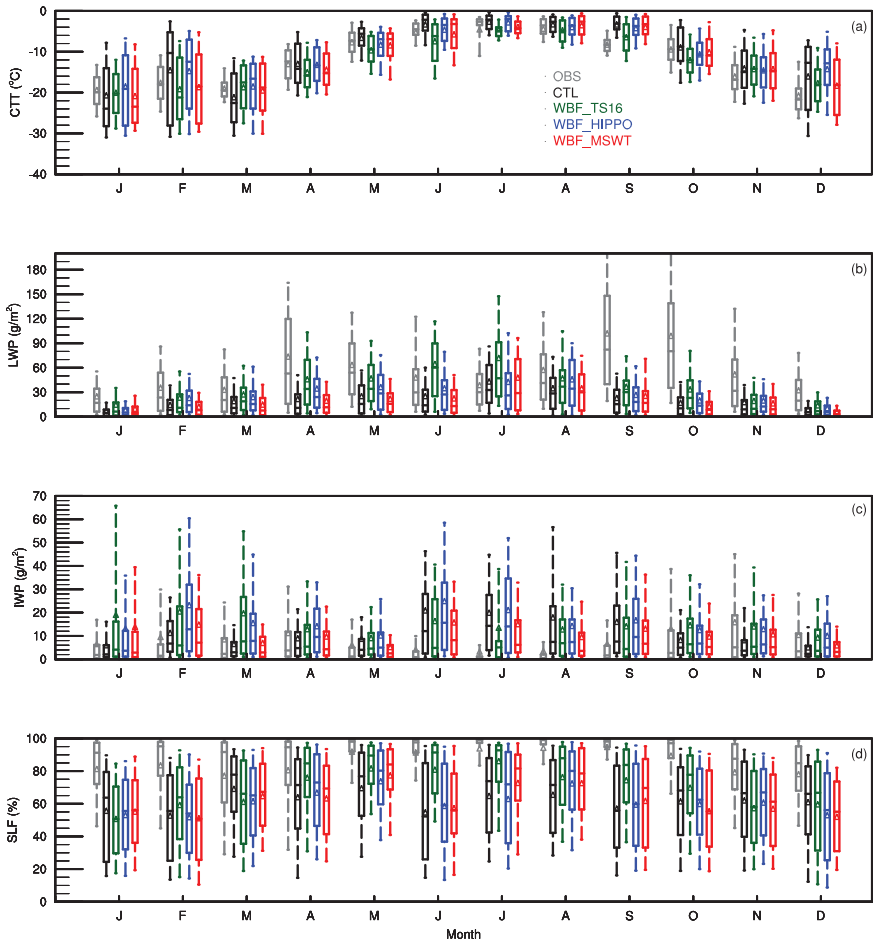

Figure 10. Monthly statistics of observed stratiform mixed-phase clouds and modeled low-level mixed-phase clouds at Barrow: (a) CTT, (b) LWP, (c) IWP, and (d) SLF. The box-and-whisker plots provide 10th, 25th, 50th, 75th, and 90th percentiles of the monthly statistics, and the means are indicated by triangles. Gray color represents the observation, while black for CTL, green for WBF_TS16, blue for WBF_HIPPO, and red for WBF_MSWT.

temperature (CTT) tends to become lower in perturbed simulations. The frequency of occurrence of low-level mixed-phase clouds indicates an insignificant sensitivity to the perturbation magnitude on the WBF process.

5.2. Cloud Properties

The observed cloud properties were obtained from long-term ground-based radar and lidar measurements at the Barrow site. Monthly LWP and IWP were derived following Wang and Sassen (2002) only for single-layer mixed-phase clouds. Figure 10 compares the monthly statistics of CTT, LWP, IWP, and SLF of low-level mixed-phase clouds between model simulations and observations. We note that due to the coarse vertical resolution, CTT sampled from model is the cloud layer temperature. As shown in Figure 10a, observed CTT has a strong seasonal variation at Barrow with warmer CTTs during the warm season (i.e., JJA). CTL generally overestimates the observed CTT especially in the boreal fall. With the perturbations in WBF process, all the three sensitivity tests alleviate the overestimation of CTT compared to CTL. The CTT decreasing extent tends to linearly relate to the perturbation magnitude, as WBF_TS16 shows the largest decrease, while WBF_HIPPO is the least and WBF_MSWT in the middle. Observed single-layer mixed-phase clouds exhibit the local maximum LWP in early boreal fall. However, all the simulations generally underestimate the observed LWP throughout the year and misrepresent the LWP peak in the boreal summer. Compared to CTL, the LWP seasonal variation becomes stronger with the introduction of mixed-phase cloud heterogeneity. WBF_TS16 indicates the most significant increase in simulated LWP of low-level mixed-phase clouds, and the remaining discrepancy from observations may be partially attributed to the inconsistent

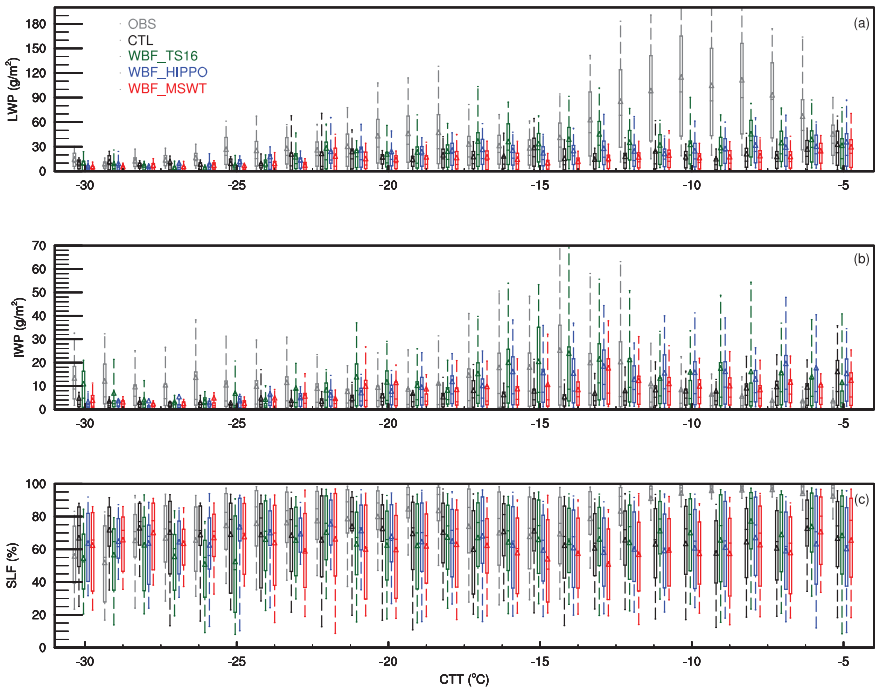

Figure 11. Statistics of observed single-layer stratiform mixed-phase cloud (gray) as a function of CTT and modeled low-level mixed-phase clouds from CTL (black) and sensitivity experiments (green, WBF_TS16; blue, WBF_HIPPO; and red, WBF_MSWT) at Barrow. (a)–(c) are for LWP, IWP, and SLF, respectively. The box-and-whisker plots are the same as in Figure 10.

treatment in cloud microphysics as revealed in section 4.3. We note that the underestimation of LWP may also be explained by the underestimated occurrence of large LWP, whereas the occurrence of low LWP is largely overestimated in modeled clouds (shown in Figure S5). In addition to the large overestimation of IWP, an opposite seasonality of IWP in low-level mixed-phase clouds is simulated in CAM5 compared to observations. For example, minimum IWP is observed in the boreal summer, but the model generates the maximum IWP for the same time period. The too high IWP during the summer can be explained by the cold bias in simulated cloud temperature. Moreover, WBF_TS16 and WBF_MSWT slightly reduce the IWP difference between boreal summer and winter, but the IWP bias in wintertime is moderately enhanced. In terms of SLF, the supercooled liquid in low-level mixed-phase clouds dominates throughout the year in observations. SLF is higher than 80% in most of the observed stratiform mixed-phase clouds at the Barrow site; and boreal summer shows the higher SLF than other seasons. Compared to the observation, simulated SLF in low-level mixed-phase clouds is largely underestimated in CTL. Slight improvements are shown in WBF_TS16 and WBF_MSWT for summer due to the reduced overestimation of IWP in these two tests, improving the modeled seasonality of SLF.

To better understand how the perturbation of WBF process would impact SLF in mixed-phase clouds, Figure 11 shows the statistics of low-level mixed-phase clouds at different CTTs at Barrow. Figure 11a indicates that LWP has a maximum centered at $-10°C$ and a minimum near $-15°C$. The minimum in LWP around $-15°C$ could be associated with the fast ice depositional growth that effectively consumes the supercooled liquid water (Korolev, 2008). The rapid ice growth at this temperature range can be demonstrated in Figure 11b in which IWP indicates a peak centered at $-14°C$. The CTL and three sensitivity experiments exhibit small differences in the relation between LWP and CTT. However, the IWP maximum near $-14°C$ is reasonably captured by WBF_TS16, WBF_HIPPO, and WBF_MSWT, implying the importance of accurate treatment of WBF process in controlling the ice phase microphysics in modeled mixed-phase clouds. Figure 11c shows a pronounced minimum in observed SLF near −15°C owing to the fast ice depositional growth through WBF process. However, none of the model experiments is able to produce this

temperature-dependent relation in SLF, because of the underestimation of LWP at temperatures between $-25°C$ and $-20°C$ and warmer than $-15°C$.

6. Summary and Conclusions

In this study, we test three different treatments of heterogeneous distribution between liquid droplets and ice crystals in mixed-phase clouds in CAM5: (1) following Tan and Storelvmo (2016), a constant perturbation magnitude of 10^6 is applied to the WBF process calculation to mimic the pocket structure of pure liquid and pure ice, in which pockets with the size of 100 m are uniformly distributed inside mixed-phase clouds; (2) mixed-phase cloud volume with co-existing liquid and ice occupies a fraction of cloud area. A perturbation factor of 0.15 based on the HIPPO analysis is used in the WBF calculation; and (3) following Fu and Hollars (2004), the mass-weighted water vapor mixing ratio is used to replace the original saturation water vapor mixing ratio with respect to liquid in the WBF calculation. The phase partitioning of modeled Arctic mixed-phase clouds in response to the perturbation of WBF process from both SCM and global simulations is compared against ground-based remote sensing observations. Observed macro- and microphysical properties of Arctic mixed-phase clouds are obtained at the ARM NSA Barrow site, covering the M-PACE field campaign in October 2004 and 2013–2017.

CAM5 sensitivity experiments indicate that a significant reduction in the WBF process rate with the introduction of cloud heterogeneity between liquid and ice enables an increase in the supercooled liquid water of Arctic mixed-phase clouds. For the M-PACE case study, simulated cloud liquid phase is largely improved, while there is no significant change in ice phase. The improvement of simulated cloud water phase partitioning tends to be linearly proportional to the perturbation magnitude that is applied to the WBF process. When comparing WBF_TS16 with WBF_HIPPO and WBF_MSWT, a larger increase in LWC is associated with a stronger reduction in the WBF process rate. Through the budget analysis of process tendencies, we find that with the WBF process perturbation, liquid water detrained from the shallow convection is enhanced due to the interactions between cloud microphysics and other physical processes. Although the conversion from liquid to ice via WBF process is inhibited, other ice phase processes such as the accretion of liquid by snow become more effective to compensate the decreased ice source from WBF process, which explains the little change in ice phase. The compensation of total IWC from snow accretion is most substantial in WBF_TS16 where the WBF processes are strictly shut down when compared to the other two sensitivity experiments. Through a consistent modification in the accretion process due to the cloud heterogeneity, further improvement is found in mixed-phase cloud partitioning. We therefore note the importance of a consistent treatment in all the cloud microphysical processes regarding the representation of heterogeneous structures of cloud hydrometeors in mixed-phase clouds. In terms of the seasonality of modeled Arctic mixed-phase cloud properties at Barrow, compared to CTL, the frequency of occurrence of low-level mixed-phase clouds shows large enhancements in boreal spring and fall, while mixed-phase clouds tend to become less frequent during the boreal summer with the perturbed WBF process. Modeled CTT and SLF exhibit larger improvements for boreal summer than other seasons in all the sensitivity experiments due to the reduced high bias in IWP, and WBF_TS16 shows the most predominant SLF improvement compared with WBF_HIPPO and WBF_MSWT. On the other hand, the temperature dependence of IWP on CTT is better captured in all the three sensitivity experiments.

Among all three sensitivity experiments, we notice that the simulated cloud macrophysical properties such as cloud fraction and frequency of occurrence of low-level mixed-phase clouds are less sensitive to the perturbation magnitude of the WBF process than cloud microphysical properties such as LWP. As the WBF process in current CAM5 is too effective to maintain cloud liquid water in mixed-phase clouds, we advocate a more physically based representation of heterogeneous structure rather than a tunable parameter, which will help to improve the phase partitioning of the Arctic mixed-phase clouds. The improved model physics better represents what actually happens by simulating the consequence of heterogeneous distribution of cloud hydrometeors on the WBF process. Since significant moisture biases are found to be related to the biased large-scale forcing, future work is advocated to address a similar microphysics problem but in a less-biased forcing framework. Additionally, other mechanisms for reducing the sink of supercooled liquid water through vapor deposition/WBF processes, i.e., ice particle size distribution changes (Harrington et al., 1999; Jiang et al., 2000; Morrison & Pinto, 2006; Pinto, 1998; Solomon et al., 2009), ice nucleation changes

(Fridlind et al., 2012; Xie et al., 2013), or by increasing the source of liquid water, i.e., due to turbulence (Furtado et al., 2016), should be pursued to accurately simulate the phase partitioning in mixed-phase clouds. Moreover, consistent with Barrett et al. (2017b), this study also finds the importance of high model vertical resolution for maintaining the liquid water in mixed-phase clouds.

Acknowledgments
X. Liu, Z. Wang and M. Zhang would like to acknowledge the support of the U.S. Department of Energy (DOE)'s Atmospheric System Research Program (grants DE-SC0014239 and DE-SC0018926). Work at LLNL was performed under the auspices of the U. S. DOE by Lawrence Livermore National Laboratory under contract No. DE-AC52-07NA27344. M. Diao acknowledges the support of the U.S. National Science Foundation (grant NSF AGS-1642291 and grant NSF OPP-1744965). D. Zhang acknowledges the support of the U.S. DOE under grant DE-SC0012704. Authors would like to acknowledge the use of computational resources (doi:10.5065/D6RX99HX) at the NCAR-Wyoming Supercomputing Center provided by the National Science Foundation and the State of Wyoming and supported by NCAR's Computational and Information Systems Laboratory. We thank the helpful comments on Fast 2-DC probe by Aaron Bansemer. The ERA-Interim reanalysis data can be downloaded from website (www.ecmwf.int). The ARM dataset is available from DOE ARM website (https://www.archive.arm.gov/discovery/). The CAM5 simulation outputs for this study are available online (https:/doi.org/10.5281/zenodo.3438437).

References

Barrett, A. I., Hogan, R. J., & Forbes, R. M. (2017a). Why are mixed-phase altocumulus clouds poorly predicted by large-scale models? Part 1. Physical processes. *Journal of Geophysical Research: Atmospheres*, *122*, 9903–9926. https://doi.org/10.1002/2016JD026321

Barrett, A. I., Hogan, R. J., & Forbes, R. M. (2017b). Why are mixed-phase altocumulus clouds poorly predicted by large-scale models? Part 2. Vertical resolution sensitivity and parameterization. *Journal of Geophysical Research: Atmospheres*, *122*, 9927–9944. https://doi.org/10.1002/2016JD026322

Bennartz, R., Shupe, M. D., Turner, D. D., Walden, V. P., Steffen, K., Cox, C. J., et al. (2013). July 2012 Greenland melt extent enhanced by low-level liquid clouds. *Nature*, *496*(7443), 83–86. https://doi.org/10.1038/nature12002

Bretherton, C. S., & Park, S. (2009). A new moist turbulence parameterization in the Community Atmosphere Model. *Journal of Climate*, *22*(12), 3422–3448. https://doi.org/10.1175/2008JCLI2556.1

Brown, P. R. A., & Francis, P. N. (1995). Improved measurements of the ice water content in cirrus using a total-water probe. *Journal of Atmospheric and Oceanic Technology*, *12*(2), 410–414. https://doi.org/10.1175/1520-0426(1995)012<0410:IMOTIW>2.0.CO;2

Chen, J. P., Hazra, A., & Levin, Z. (2008). Parameterizing ice nucleation rates using contact angle and activation energy derived from laboratory data. *Atmospheric Chemistry and Physics*, *8*(24), 7431–7449. https://doi.org/10.5194/acp-8-7431-2008

Clothiaux, E. E., Ackerman, T. P., Mace, G. G., Moran, K. P., Marchand, R. T., Miller, M. A., & Martner, B. E. (2000). Objective determination of cloud heights and radar reflectivities using a combination of active remote sensors at the ARM CART sites. *Journal of Applied Meteorology and Climatology*, *39*(5), 645–665. https://doi.org/10.1175/1520-0450(2000)039<0645:ODOCHA>2.0.CO;2

D'Alessandro, J. J., Diao, M., Wu, C., Liu, X., Jensen, J. B., & Stephens, B. B. (2019). Cloud phase and relative humidity distributions over the Southern Ocean in austral summer based on in situ observations and CAM5 simulations. *Journal of Climate*, *32*(10), 2781–2805. https://doi.org/10.1175/JCLI-D-18-0232.1

de Boer, G., Eloranta, E. W., & Shupe, M. D. (2009). Arctic mixed-phase stratiform cloud properties from multiple years of surface-based measurements at two high-latitude locations. *Journal of the Atmospheric Sciences*, *66*(9), 2874–2887. https://doi.org/10.1175/2009JAS3029.1

DeMott, P. J., Prenni, A. J., Liu, X., Kreidenweis, S. M., Petters, M. D., Twohy, C. H., et al. (2010). Predicting global atmospheric ice nuclei distributions and their impacts on climate. *Proceedings of the National Academy of Sciences*, *107*(25), 11 217–11 222. https://doi.org/10.1073/pnas.0910818107

DeMott, P. J., Prenni, A. J., McMeeking, G. R., Sullivan, R. C., Petters, M. D., Tobo, Y., et al. (2015). Integrating laboratory and field data to quantify the immersion freezing ice nucleation activity of mineral dust particles. *Atmospheric Chemistry and Physics*, *15*(1), 393–409. https://doi.org/10.5194/acp-15-393-2015

Fan, J., Ghan, S., Ovchinnikov, M., Liu, X., Rasch, P. J., & Korolev, A. (2011). Representation of Arctic mixed-phase clouds and the Wegener-Bergeron-Findeisen process in climate models: Perspectives from a cloud-resolving study. *Journal of Geophysical Research: Atmospheres*, *116*, D00T07. https://doi.org/10.1029/2010JD015375

Field, P. R., Lawson, R. P., Brown, P. R., Lloyd, G., Westbrook, C., Moisseev, D., et al. (2017). Secondary ice production: Current state of the science and recommendations for the future. *Meteorological Monographs*, *58*, 7.1–7.20. https://doi.org/10.1175/AMSMONOGRAPHS-D-16-0014.1

Fridlind, A. M., van Diedenhoven, B., Ackerman, A. S., Avramov, A., Mrowiec, A., Morrison, H., et al. (2012). A FIRE-ACE/SHEBA case study of mixed-phase Arctic boundary layer clouds: Entrainment rate limitations on rapid primary ice nucleation processes. *Journal of the Atmospheric Sciences*, *69*(1), 365–389. https://doi.org/10.1175/JAS-D-11-052.1

Fu, Q., & Hollars, S. (2004). Testing mixed-phase cloud water vapor parameterizations with SHEBA/FIRE-ACE observations. *Journal of the Atmospheric Sciences*, *61*(16), 2083–2091. https://doi.org/10.1175/1520-0469(2004)061<2083:TMCWVP>2.0.CO;2

Furtado, K., Field, P. R., Boutle, I. A., Morcrette, C. J., & Wilkinson, J. M. (2016). A physically based subgrid parameterization for the production and maintenance of mixed-phase clouds in a general circulation model. *Journal of the Atmospheric Sciences*, *73*(1), 279–291. https://doi.org/10.1175/JAS-D-15-0021.1

Fyfe, J. C., Von Salzen, K., Gillett, N. P., Arora, V. K., Flato, G. M., & McConnell, J. R. (2013). One hundred years of Arctic surface temperature variation due to anthropogenic influence. *Scientific Reports*, *3*(1), 2645. https://doi.org/10.1038/srep02645

Garrett, T. J., & Zhao, C. (2006). Increased Arctic cloud longwave emissivity associated with pollution from mid-latitudes. *Nature*, *440*(7085), 787–789. https://doi.org/10.1038/nature04636

Harrington, J. Y., Reisin, T., Cotton, W. R., & Kreidenweis, S. M. (1999). Cloud resolving simulations of Arctic stratus: Part II: Transition-season clouds. *Atmospheric Research*, *51*(1), 45–75. https://doi.org/10.1016/S0169-8095(98)00098-2

Hartmann, D. L., Klein Tank, A. M. G., Rusticucci, M., Alexander, L. V., Brönnimann, S., Charabi, Y., et al. (2013). Observations: Atmosphere and surface. In Climate Change 2013: The Physical Science Basis. In *Contribution of Working Group I to the Fifth Assessment Report of the Intergovernmental Panel on Climate Change* (pp. 159–254). Cambridge, United Kingdom and New York, NY, USA: Cambridge University Press.

Hofer, S., Tedstone, A. J., Fettweis, X., & Bamber, J. L. (2019). Cloud microphysics and circulation anomalies control differences in future Greenland melt. *Nature Climate Change*, *9*(7), 523–528. https://doi.org/10.1038/s41558-019-0507-8

Hoose, C., Kristjánsson, J. E., Chen, J. P., & Hazra, A. (2010). A classical-theory-based parameterization of heterogeneous ice nucleation by mineral dust, soot, and biological particles in a global climate model. *Journal of the Atmospheric Sciences*, *67*(8), 2483–2503. https://doi.org/10.1175/2010JAS3425.1

Huang, J., Zhang, X., Zhang, Q., Lin, Y., Hao, M., Luo, Y., et al. (2017). Recently amplified arctic warming has contributed to a continual global warming trend. *Nature Climate Change*, *7*(12), 875–879. https://doi.org/10.1038/s41558-017-0009-5

Iacono, M. J., Delamere, J. S., Mlawer, E. J., Shephard, M. W., Clough, S. A., & Collins, W. D. (2008). Radiative forcing by long-lived greenhouse gases: Calculations with the AER radiative transfer models. *Journal of Geophysical Research: Atmospheres*, *113*, D13103. https://doi.org/10.1029/2008JD009944

Jiang, H., Cotton, W. R., Pinto, J. O., Curry, J. A., & Weissbluth, M. J. (2000). Cloud resolving simulations of mixed-phase Arctic stratus observed during BASE: Sensitivity to concentration of ice crystals and large-scale heat and moisture advection. *Journal of the Atmospheric Sciences*, *57*(13), 2105–2117. https://doi.org/10.1175/1520-0469(2000)057<2105:CRSOMP>2.0.CO;2

Khanal, S., & Wang, Z. (2015). Evaluation of the lidar-radar cloud ice water content retrievals using collocated in situ measurements. *Journal of Applied Meteorology and Climatology*, *54*(10), 2087–2097. https://doi.org/10.1175/JAMC-D-15-0040.1

Klein, S. A., McCoy, R. B., Morrison, H., Ackerman, A. S., Avramov, A., de Boer, G., et al. (2009). Intercomparison of model simulations of mixed-phase clouds observed during the ARM Mixed-Phase Arctic Cloud Experiment. I: single-layer cloud. *Quarterly Journal of the Royal Meteorological Society*, *135*(641), 979–1002. https://doi.org/10.1002/qj.416

Korolev, A. (2007). Limitations of the Wegener-Bergeron-Findeisen mechanism in the evolution of mixed-phase clouds. *Journal of the Atmospheric Sciences*, *64*(9), 3372–3375. https://doi.org/10.1175/JAS4035.1

Korolev, A., & Field, P. R. (2008). The effect of dynamics on mixed-phase clouds: Theoretical considerations. *Journal of the Atmospheric Sciences*, *65*(1), 66–86. https://doi.org/10.1175/2007JAS2355.1

Korolev, A., & Isaac, G. A. (2006). Relative humidity in liquid, mixed-phase, and ice clouds. *Journal of the Atmospheric Sciences*, *63*(11), 2865–2880. https://doi.org/10.1175/JAS3784.1

Korolev, A., McFarquhar, G., Field, P. R., Franklin, C., Lawson, P., Wang, Z., et al. (2017). Mixed-phase clouds: Progress and challenges. *Meteorological Monographs*, *58*, 5.1–5.50. https://doi.org/10.1175/AMSMONOGRAPHS-D-17-0001.1

Korolev, A. V. (2008). Rates of phase transformations in mixed-phase clouds. *Quarterly Journal of the Royal Meteorological Society*, *134*(632), 595–608. https://doi.org/10.1002/qj.230

Korolev, A. V., Isaac, G. A., Cober, S. G., Strapp, J. W., & Hallett, J. (2003). Microphysical characterization of mixed-phase clouds. *Quarterly Journal of the Royal Meteorological Society*, *129*(587), 39–65. https://doi.org/10.1256/qj.01.204

Korolev, A. V., & Mazin, I. P. (2003). Supersaturation of water vapor in clouds. *Journal of the Atmospheric Sciences*, *60*(24), 2957–2974. https://doi.org/10.1175/1520-0469(2003)060<2957:SOWVIC>2.0.CO;2

Liu, X., Easter, R. C., Ghan, S. J., Zaveri, R., Rasch, P., Shi, X., et al. (2012). Toward a minimal representation of aerosols in climate models: Description and evaluation in the Community Atmosphere Model CAM5. *Geoscientific Model Development*, *5*(3), 709–739. https://doi.org/10.5194/gmd-5-709-2012

Liu, X., Xie, S., Boyle, J., Klein, S. A., Shi, X., Wang, Z., et al. (2011). Testing cloud microphysics parameterizations in NCAR CAM5 with ISDAC and M-PACE observations. *Journal of Geophysical Research: Atmospheres*, *116*, D00T11. https://doi.org/10.1029/2011JD015889

Liu, X., Xie, S., & Ghan, S. J. (2007). Evaluation of a new mixed-phase cloud microphysics parameterization with CAM3 single-column model and M-PACE observations. *Geophysical Research Letters*, *34*, L23712. https://doi.org/10.1029/2007GL031446

Lord, S. J., Willoughby, H. E., & Piotrowicz, J. M. (1984). Role of a parameterized ice-phase microphysics in an axisymmetric, nonhydrostatic tropical cyclone model. *Journal of the Atmospheric Sciences*, *41*(19), 2836–2848. https://doi.org/10.1175/1520-0469(1984)041<2836:ROAPIP>2.0.CO;2

McCoy, D. T., Hartmann, D. L., Zelinka, M. D., Ceppi, P., & Grosvenor, D. P. (2015). Mixed-phase cloud physics and Southern Ocean cloud feedback in climate models. *Journal of Geophysical Research: Atmospheres*, *120*, 9539–9554. https://doi.org/10.1002/2015JD023603

McCoy, D. T., Tan, I., Hartmann, D. L., Zelinka, M. D., & Storelvmo, T. (2016). On the relationships among cloud cover, mixed-phase partitioning, and planetary albedo in GCMs. *Journal of Advances in Modeling Earth Systems*, *8*, 650–668. https://doi.org/10.1002/2015MS000589

Meyers, M. P., DeMott, P. J., & Cotton, W. R. (1992). New primary ice-nucleation parameterizations in an explicit cloud model. *Journal of Applied Meteorology and Climatology*, *31*(7), 708–721. https://doi.org/10.1175/1520-0450(1992)031<0708:NPINPI>2.0.CO;2

Morrison, H., de Boer, G., Feingold, G., Harrington, J., Shupe, M. D., & Sulia, K. (2012). Resilience of persistent Arctic mixed-phase clouds. *Nature Geoscience*, *5*(1), 11–17. https://doi.org/10.1038/ngeo1332

Morrison, H., & Gettelman, A. (2008). A new two-moment bulk stratiform cloud microphysics scheme in the Community Atmosphere Model version 3 (CAM3). Part I: Description and numerical tests. *Journal of Climate*, *21*(15), 3642–3659. https://doi.org/10.1175/2008JCLI2105.1

Morrison, H., McCoy, R. B., Klein, S. A., Xie, S., Luo, Y., Avramov, A., et al. (2009). Intercomparison of model simulations of mixed-phase clouds observed during the ARM mixed-phase Arctic Cloud Experiment. II: Multilayer cloud. *Quarterly Journal of the Royal Meteorological Society*, *135*(641), 1003–1019. https://doi.org/10.1002/qj.415

Morrison, H., & Pinto, J. O. (2006). Intercomparison of bulk cloud microphysics schemes in mesoscale simulations of springtime Arctic mixed-phase stratiform clouds. *Monthly Weather Review*, *134*(7), 1880–1900. https://doi.org/10.1175/MWR3154.1

Neale, R. B., Chen, C. C., Gettelman, A., Lauritzen, P. H., Park, S., Williamson, D. L., et al. (2010). *Description of the NCAR community atmosphere model* (CAM 5.0) (NCAR/TN-4861STR). Boulder, CO: National Center for Atmospheric Research. http://www.cesm.ucar.edu/models/cesm1.2/cam/docs/description/cam5_desc.pdf

Park, S., & Bretherton, C. S. (2009). The University of Washington shallow convection and moist turbulence schemes and their impact on climate simulations with the Community Atmosphere Model. *Journal of Climate*, *22*(12), 3449–3469. https://doi.org/10.1175/2008JCLI2557.1

Pinto, J. O. (1998). Autumnal mixed-phase cloudy boundary layers in the Arctic. *Journal of the Atmospheric Sciences*, *55*(11), 2016–2038. https://doi.org/10.1175/1520-0469(1998)055<2016:AMPCBL>2.0.CO;2

Pithan, F., & Mauritsen, T. (2014). Arctic amplification dominated by temperature feedbacks in contemporary climate models. *Nature Geoscience*, *7*(3), 181–184. https://doi.org/10.1038/ngeo2071

Prenni, A. J., Harrington, J. Y., Tjernström, M., DeMott, P. J., Avramov, A., Long, C. N., et al. (2007). Can ice-nucleating aerosols affect arctic seasonal climate? *Bulletin of the American Meteorological Society*, *88*(4), 541–550. https://doi.org/10.1175/BAMS-88-4-541

Screen, J. A., & Simmonds, I. (2010). The central role of diminishing sea ice in recent Arctic temperature amplification. *Nature*, *464*(7293), 1334–1337. https://doi.org/10.1038/nature09051

Shupe, M. D. (2011). Clouds at Arctic atmospheric observatories. Part II: Thermodynamic phase characteristics. *Journal of Applied Meteorology and Climatology*, *50*(3), 645–661. https://doi.org/10.1175/2010JAMC2468.1

Shupe, M. D., Kollias, P., Persson, P. O. G., & McFarquhar, G. M. (2008). Vertical motions in Arctic mixed-phase stratiform clouds. *Journal of the Atmospheric Sciences*, *65*(4), 1304–1322. https://doi.org/10.1175/2007JAS2479.1

Shupe, M. D., Matrosov, S. Y., & Uttal, T. (2006). Arctic mixed-phase cloud properties derived from surface-based sensors at SHEBA. *Journal of the Atmospheric Sciences*, *63*(2), 697–711. https://doi.org/10.1175/JAS3659.1

Solomon, A., Morrison, H., Persson, O., Shupe, M. D., & Bao, J. (2009). Investigation of microphysical parameterizations of snow and ice in Arctic clouds during M-PACE through model-observation Comparisons. *Monthly Weather Review*, *137*(9), 3110–3128. https://doi.org/10.1175/2009MWR2688.1

Storelvmo, T., Kristjánsson, J. E., Lohmann, U., Iversen, T., Kirkevåg, A., & Seland, Ø. (2008). Modeling of the Wegener-Bergeron-Findeisen process—implications for aerosol indirect effects. *Environmental Research Letters*, *3*(4), 045001. https://doi.org/10.1088/1748-9326/3/4/045001

Tan, I., & Storelvmo, T. (2016). Sensitivity study on the influence of cloud microphysical parameters on mixed-phase cloud thermodynamic phase partitioning in CAM5. *Journal of the Atmospheric Sciences*, *73*(2), 709–728. https://doi.org/10.1175/JAS-D-15-0152.1

Tan, I., Storelvmo, T., & Zelinka, M. D. (2016). Observational constraints on mixed-phase clouds imply higher climate sensitivity. *Science*, *352*(6282), 224–227. https://doi.org/10.1126/science.aad5300

Verlinde, J., Harrington, J. Y., McFarquhar, G. M., Yannuzzi, V. T., Avramov, A., Greenberg, S., et al. (2007). The mixed-phase Arctic Cloud Experiment. *Bulletin of the American Meteorological Society*, *88*(2), 205–222. https://doi.org/10.1175/BAMS-88-2-205

Wang, Y., Liu, X., Hoose, C., & Wang, B. (2014). Different contact angle distributions for heterogeneous ice nucleation in the Community Atmospheric Model version 5. *Atmospheric Chemistry and Physics*, *14*(19), 10 411–10 430. https://doi.org/10.5194/acp-14-10411-2014

Wang, Y., Zhang, D., Liu, X., & Wang, Z. (2018). Distinct contributions of ice nucleation, large-scale environment, and shallow cumulus detrainment to cloud phase partitioning with NCAR CAM5. *Journal of Geophysical Research: Atmospheres*, *123*(2), 1132–1154. https://doi.org/10.1002/2017JD027213

Wang, Z. (2007). A refined two-channel microwave radiometer liquid water path retrieval for cold regions by using multiple-sensor measurements. *IEEE Geoscience and Remote Sensing Letters*, *4*(4), 591–595. https://doi.org/10.1109/LGRS.2007.900752

Wang, Z., & Sassen, K. (2002). Cirrus cloud microphysical property retrieval using lidar and radar measurements. Part I: Algorithm description and comparison with in situ data. *Journal of Applied Meteorology and Climatology*, *41*(3), 218–229. https://doi.org/10.1175/1520-0450(2002)041<0218:CCMPRU>2.0.CO;2

Wofsy, S. C., Daube, B. C., Jimenez, R., Kort, E., Pittman, J. V., Park, S., et al. (2011). HIAPER Pole-to-Pole Observations (HIPPO): fine-grained, global-scale measurements of climatically important atmospheric gases and aerosols. *Philosophical Transactions of the Royal Society A*, *369*(1943), 2073–2086. https://doi.org/10.1098/rsta.2010.0313

Wood, R., & Field, P. R. (2000). Relationships between Total Water, Condensed Water, and Cloud Fraction in Stratiform Clouds Examined Using Aircraft Data. *Journal of the Atmospheric Sciences*, *57*(12), 1888–1905. https://doi.org/10.1175/1520-0469(2000)057<1888:RBTWCW>2.0.CO;2

Xie, S., Boyle, J., Klein, S. A., Liu, X., & Ghan, S. (2008). Simulations of Arctic mixed-phase clouds in forecasts with CAM3 and AM2 for M-PACE. *Journal of Geophysical Research: Atmospheres*, *113*, D04211. https://doi.org/10.1029/2007JD009225

Xie, S., Klein, S. A., Yio, J. J., Beljaars, A. C. M., Long, C. N., & Zhang, M. (2006). An assessment of ECMWF analyses and model forecasts over the North Slope of Alaska using observations from the ARM mixed-phase Arctic Cloud Experiment. *Journal of Geophysical Research: Atmospheres*, *111*, D05107. https://doi.org/10.1029/2005JD006509

Xie, S., Liu, X., Zhao, C., & Zhang, Y. (2013). Sensitivity of CAM5-simulated Arctic Clouds and radiation to ice nucleation parameterization. *Journal of Climate*, *26*(16), 5981–5999. https://doi.org/10.1175/JCLI-D-12-00517.1

Xie, S., Zhang, M., Branson, M., Cederwall, R. T., Del Genio, A. D., Eitzen, Z. A., et al. (2005). Simulations of midlatitude frontal clouds by single-column and cloud-resolving models during the Atmospheric Radiation Measurement March 2000 cloud intensive operational period. *Journal of Geophysical Research: Atmospheres*, *110*(D15), D15S03. https://doi.org/10.1029/2004JD005119

Yuan, J., Fu, Q., & McFarlane, N. (2006). Tests and improvements of GCM cloud parameterizations using the CCCMA SCM with the SHEBA data set. *Atmospheric Research*, *82*(1-2), 222–238. https://doi.org/10.1016/j.atmosres.2005.10.009

Zhang, D., Vogelmann, A., Kollias, P., Luke, E., Yang, F., Lubin, D., & Wang, Z. (2019). Comparison of Antarctic and Arctic single-layer stratiform mixed-phase cloud properties using ground-based remote sensing measurements. *Journal of Geophysical Research: Atmospheres*, *124*(17-18), 10 186–10 204. https://doi.org/10.1029/2019JD030673

Zhang, D., Wang, Z., Heymsfield, A., Fan, J., & Luo, T. (2014). Ice concentration retrieval in stratiform mixed-phase clouds using cloud radar reflectivity measurements and 1D ice growth model simulations. *Journal of the Atmospheric Sciences*, *71*(10), 3613–3635. https://doi.org/10.1175/JAS-D-13-0354.1

Zhang, G. J., & McFarlane, N. A. (1995). Sensitivity of climate simulations to the parameterization of cumulus convection in the Canadian Climate Centre general circulation model. *Atmosphere-Ocean*, *33*(3), 407–446. https://doi.org/10.1080/07055900.1995.9649539